NATIONAL
OPTICAL
ASTRONOMY
OBSERVATORIES

Preprint Series

NOAO Preprint No. 828

Chemical Abundances of Planetary Nebulae In the Bulge and Disk of M31

George H. Jacoby
Robin Ciardullo

Accepted by: The Astrophysical Journal

December 1998

Operated for the National Science Foundation by the Association of Universities for Research in Astronomy, Inc.

Chemical Abundances of Planetary Nebulae in the Bulge and Disk of M31

George H. Jacoby[1]
Kitt Peak National Observatory, National Optical Astronomy Observatories,
P.O. Box 26732, Tucson, AZ, 85726

Robin Ciardullo[2]
Department of Astronomy and Astrophysics, Penn State University, 525 Davey Lab, University Park, PA 16802

ABSTRACT

We derive abundances and central star parameters for 15 planetary nebulae (PNe) in M31: 12 in the bulge and 3 in a disk field 14 kpc from the nucleus. No single abundance value characterizes the bulge stars: although the median abundances of the sample are similar to those seen for PNe in the LMC, the distribution of abundances is several times broader, spanning over 1 decade. None of the PNe in our sample approach the super metal-rich ([Fe/H] $\sim +0.25$) expectations for the bulge of M31, although a few PNe in the sample of Stasińska, Richer, & Mc Call (1998) come close. This [O/H] vs [Fe/H] discrepancy is likely due to a combination of factors, including an inability of metal-rich stars to produce bright PNe, a luminosity selection effect, and an abundance gradient in the bulge of M31. We show that PNe that are near the bright limit of the [O III] λ5007 planetary nebula luminosity function (PNLF) span nearly a decade in oxygen abundance, and thus, support the use of the PNLF for deriving distances to galaxies (Jacoby 1996) with differing metallicities. We also identify a correlation between central star mass and PN dust formation that partially alleviates any dependence of the PNLF maximum magnitude on population age. Additionally, we identify a spatially compact group of 5 PNe having unusually high O/H; this subgroup may arise from a recent merger, but velocity information is needed to assess the true nature of the objects.

Subject headings: galaxies: individual (M31) — planetary nebulae: general — stars: abundances — stars: AGB and post-AGB — stars: evolution

---

[1]Visiting Astronomer, Steward Observatory, University of Arizona, 933 N. Cherry Ave, Tucson, AZ 85721

[2]Visiting Astronomer, Kitt Peak National Observatory, National Optical Astronomy Observatories, which is operated by the Association of Universities for Research in Astronomy, Inc., under cooperative agreement with the National Science Foundation.

1. Introduction

Ever since the pioneering work by Spinrad & Taylor (1971) on the optical spectra of M31's bulge, the evidence from integrated spectroscopy has been that the cores of giant E/S0 galaxies and the bulges of large spirals contain a significant population of metal-enriched stars (e.g., Bica, Alloin, & Schmidt 1990; Worthey, Faber, & Gonzalez 1992 (WFG); Davies, Sadler, & Peletier 1993; Carollo, Danziger, & Buson 1993; Vazdekis et al. 1997). For example, WFG reaffirm the Spinrad & Taylor (1971) result that the stars in the bulge of M31 have [Fe/H] $\sim$ +0.23, i.e., a value 70% higher than the Sun.

On the other hand, Ferguson et al. (1991) have shown that the very weak lines in the UV upturn of NGC 1399 are consistent with the existence of a metal-poor population mixed-in with the metal-rich stars. This idea is confirmed is M32, where the color-magnitude diagram of Freedman (1989) demonstrates a large range ($\sim$ 0.6 dex) in the metallicity of the stars, and the HST results by Grillmair et al. (1996) confirm an even wider range ($\sim$ 1.1 dex). Furthermore, studies of the stars in the bulge of our own Galaxy have shown that there can be large abundance variations from star to star, and that extreme care must be taken when interpretating even these relatively simple data (see review by McWilliam 1997). Given this complication, our ability to investigate the chemistry of galaxies via integrated spectroscopy seems limited. Instead, studies of large numbers of individual stars are preferred.

Planetary nebulae (PNe) are excellent tools for obtaining both the mean metallicity and metallicity dispersion within large, nearby galaxies. Because bright PNe are plentiful, large numbers of objects are available for analysis. Moreover, although internal chemical processing does affect some of a PN's constituent elements (e.g., helium, nitrogen, and carbon), important elements, such as oxygen, neon, argon, and sulfur are generally considered to be largely unaffected. Of greatest importance, however, is the presence of planetary nebulae throughout a galaxy. Because PNe do not belong to any single stellar population, they can be used to measure bulge, disk, and halo abundances via a single analysis technique. Abundance gradients can therefore be measured from the very center of the galaxy to the outermost regions in a uniform manner (cf. Jacoby & Ford 1986), rather than the mixture of techniques (absorption line measurements for bulge stars, emission line measurements for disk H II regions, broadband colors for halo stars) that are otherwise necessary.

The power of planetary nebulae to probe both the make-up and chemical history of a stellar population has been demonstrated by Dopita et al. (1997). By deriving the central star properties (T_{eff}, $L/L_{\odot}$, and $M/M_{\odot}$), and adopting an initial-to-final mass relation (e.g., Vassiliadis & Wood 1994), Dopita et al. were able to compare the alpha element abundances of LMC planetaries to the main sequence turn-off ages of their progenitors, and consequently, to trace the history of chemical enrichment within that galaxy. While mergers and infall events may confuse the issue of chemical enrichment in larger, more complex systems, the degree to which a monotonic relation between abundance and age does exist can place limits on the importance of mergers in a galaxy's

evolution.

Nevertheless, aside from observations of objects in the Magellanic Clouds, there is little spectroscopic data for extragalactic planetary nebulae. In particular, there have been only two previous studies of planetary nebulae in M31: the early efforts of Jacoby & Ford (1986), and the recent observations of Richer, Stasińska, & Mc Call (1998; hereafter RSM). The former study included only three PNe, two in the halo of M31, and one in the disk; the latter work consisted of observations of 28 bulge PNe and 2 outer disk PNe. Based on their observations, Stasińska, Richer, & Mc Call (1998; hereafter SRM) find that a very wide range of abundances exists among the M31 bulge stars, with [O/H] ranging between -1.0 and $+0.2$.

In this paper we report spectroscopic observations and model nebula analyses for 15 PNe in M31. In §2, we describe our observations and reductions; in §3, we use photoionzation models to derive abundances and central star parameters for our objects. We review the abundance results for PNe in M31's bulge and disk in §4, and we discuss the PN abundances in the context of their metal-rich environment in §5.

2. Observations and Reductions

2.1. Observing strategy

We observed 16 planetary nebulae in the bulge and disk of M31 with slit masks on the R-C spectrograph of the Kitt Peak 4-m telescope. The spectrograph configuration consisted of a 316 lines/mm grating blazed at 4000 Å in first order (KPC-10A), a WG360 blocking filter, and the T2KB 2048×2048 CCD with 24 micron pixels. This setup, combined with an atmospheric dispersion corrector and $2''$ wide slitlets (multiple, short slits, etched into a focal plane mask), enabled us to perform relative spectrophotometry over a full octave of wavelength from 3700 Å to 7400 Å, with 6.9 Å resolution at 2.75 Å per pixel. Perpendicular to dispersion, the instrument delivered a scale of $0\farcs69$ per pixel, over a slit length of $\sim 12''$. With complete optical coverage over a very large range of airmasses, this setup is very good for measuring nebular abundances; it is, however, non-optimal for deriving radial velocities because of the low dispersion and wide slit.

Observations were taken on two nights. On UT date 1995 September 20, we observed 13 of the bulge PNe identified by Ford & Jacoby (1978) and Ciardullo et al. (1989; CJFN) in their surveys of M31's bulge and inner disk. These observations consisted of 13 1800-second exposures, taken under photometric conditions with a typical seeing $\sim 0\farcs9$. The following night, we observed 3 PNe found by Ford et al. (2000; FJCHP) in their large area survey of M31's disk. These objects, which are at a projected galactocentric distance of 14 kpc, were observed via 12 1800-sec exposures taken through light cirrus and $\sim 0\farcs9$ seeing. The data of both nights were calibrated via a series of exposures of the spectrophotometric standards BD+26 3941, G191B2B, HD 192291, and BD+28 4211 (Stone 1977; Oke 1974), with the stars positioned in each slitlet at least once. A

summary of the observations appears in Table 1. Note that the PNe chosen for study span a range of 2.4 mag in the [O III] λ5007 planetary nebula luminosity function. Kaler (1995) noted that the spectra of the brightest M31 bulge PNe exhibit considerable uniformity, and so, by including fainter objects in our sample, we sought to decrease the impact of selection effects on the derived distribution of nebular abundances.

2.2. Special data reduction issues

The need for both wide wavelength coverage and accurate sky subtraction of the bright galaxy background presented a unique set of problems for the reduction of our slitlet data. The design of the R-C spectrograph is such that the instrument's focus changes at the ends of the spectral range. Consequently, the width of our spectra varied with wavelength, especially for those objects positioned near the edge of the instrument's field-of-view. The need to extract a wide, sometimes slightly out-of-focus spectrum, coupled with the limited amount of sky covered by each slitlet, prevented us from using any standard reduction method.

To reduce our spectra, we began by debiasing the raw CCD frames, and extracting the data region of each slitlet. We then created a normalized flatfield frame for each slitlet using observations of both the interior dome screen and the twilight sky. To do this, we first removed the effects of vignetting from our dome flats by fitting a high-order spline to the data, and then dividing the flatfield by this function. We applied this normalized flatfield to spectra of the twilight sky, and examined the resulting image for residual structure in the spatial direction. If any structure was apparent, we fit it with a low-order polynomial, and re-normalized the dome flat to remove the effect. Once the final, normalized dome flat was calculated, we used it to flatten all spectra taken through the slitlet.

After flatfielding the data, we carefully examined the sky spectrum surrounding each PN, paying particular attention to the nebular emission lines near Hα. As detailed by Ciardullo et al. (1988) and Jacoby, Ford, & Ciardullo (1985), the bulge of M31 contains a series of irregular emission features, whose [N II], [S II], and Hα flux can be as bright, or brighter than, the target planetary. This greatly confuses the issue of sky-subtraction, for a single knot of emission within a slitlet can cause the background at these wavelengths to be severely overestimated. To reduce this problem, we inspected the data of each slitlet, and identified any anomalously bright emission regions along our slit. If an emission knot was detected, its presence was noted and that region of the slitlet was excluded from the analysis.

Once the inspection was complete, we proceeded to extract the object spectrum from each slitlet. To do this, we used our standard star observations to trace both the shape and the varying width of the spectra produced in each slitlet. We then applied these parameters to our program objects, using the bright [O III] λ5007 line as a reference to define the exact position of the PN within the slitlet. Our extraction program defined three regions: an object region, which changed

in size along the spectrum and included $\sim 90\%$ of the object counts, and two sky regions, one on either side of the object (and separated from the target spectrum by ~ 3 pixels). Using the sky regions, we estimated the sky value underlying each pixel in the object region, either by adopting a median sky value, or, for those PNe close to the nucleus, by fitting a low-order function to the data in the spatial direction. The sky was then subtracted from the object pixels, and the object counts summed to produce a one-dimensional, sky-subtracted spectrum.

Following the sky-subtraction, the data reduction continued in a more standard manner. By dividing our exposure into ~ 12 separate 30-min frames, we were able to identify cosmic rays via a sigma-clipping algorithm: any point that was more than $\sim 10\sigma$ from the median was deleted from the analysis. A series of He-Ne-Ar comparison arcs taken throughout the night served as the wavelength calibration. Each individual spectrum was linearized, corrected for atmospheric extinction, and flux-calibrated using the comparison arcs and the observations of the spectrophotometric standard stars. Finally, the ~ 12 spectra of each PN were combined, using the number of counts recorded in the [O III] λ5007 line to weight the averaging. The final reduced spectra are shown in Figure 1 (bulge PNe) and Figure 2 (disk PNe).

2.3. Reduction to dereddened line ratios

The integrated flux in a line was derived using the Gaussian line fitting and deblending tools in the SPLOT task of IRAF. Line strengths in each spectrum were measured at least twice, to assess the subjective uncertainty in placing the continuum, which is one of the dominant sources of error for the faint lines. Typically, we found that the measurement uncertainty is roughly 2% of the strength of Hβ, except for the region near λ3727, where the system sensitivity is dropping quickly. In this region, the errors depend on the background signal relative to the PN signal, and are typically magnified by factors of 3 to 10.

The spectrum of one PN, CJFN 9, was so weak that no usable information could be extracted. We dropped that PN from our sample. The remaining 15 PNe have line strengths after dereddening (Cardelli, Clayton, & Mathis 1989) as given in Table 2. The logarithmic extinction at Hβ, c, derived from the Balmer decrement, $I(\mathrm{H}\alpha)/I(\mathrm{H}\beta)$, is also listed in the table. The uncertainty in this ratio is typically about 5%, such that $\delta c \sim 0.06$.

Table 2 also lists the absolute extinction-corrected flux, L_{5007}, of each planetary. These numbers were derived by taking the magnitudes tabulated by CJFN, and scaling them to an M31 Cepheid distance of 770 kpc (Freedman & Madore 1990). As discussed in the next section, the nebula luminosities provide an important constraint on the models, and help define the central star luminosity and mass.

3. Analysis Using Photoionization Models

As can be seen from Figures 1 and 2, the quality of some of the PN spectra are excellent: lines as faint as 10% of Hβ can be measured accurately. On the other hand, many of the spectra are missing lines such as [S II] $\lambda\lambda$6716, 6731 and [O III] λ4363, which are necessary to derive electron densities (N_e) and temperatures (T_e). In order to proceed with an abundance analysis in the latter cases, one can adopt reasonable values for these parameters (e.g., $T_e = 10,000$K; $N_e = 4,000$). Or, since the more important parameter is T_e, one can estimate an upper limit for $I(\lambda 4363)$, infer an upper limit for T_e, and consequently, derive a lower limit for the abundances of the collisionally excited elements. This latter approach was adopted by SRM in their analysis of extragalactic PNe.

Rather than use this approach, we have chosen to use the CLOUDY 90.04 photoionization code (Ferland et al. 1998) to indirectly deduce the viable range of elemental abundances using whatever emission-lines strengths (or upper limits) that are available. Though the technique is time consuming, and not necessarily suitable for large volumes of data (such as that of the SRM study), the method does have the advantage of allowing us to investigate the properties of both the nebula and the central exciting star. An intangible asset of using photoionization modeling is that the process focuses one's thinking on the physical properties (radius, luminosity, dust content, central star temperature) of each PN as a real entity rather than simply a column of line strengths.

3.1. Philosophy of the modeling process

Generally, for our sample of PNe, there were too few lines to fully constrain all aspects of a photoionization model. Consequently, we modeled each object with the simplest set of parameters possible. Complexities were added only if a viable model could not be built, where we defined a viable model as one in which a) the predicted emission-line ratios matched the observed line ratios to within 2% of I(Hβ), and b) the total [O III] λ5007 flux of the model matched the observed, dereddened flux. As a result, our basic model consisted of a hot black-body central star centered in a spherical nebula having uniform density and containing dust grains typical of most PNe. In two cases the uniform density assumption failed, and a multizone model was needed, in six cases dust was omitted from the nebula, and, in one difficult case (CJFN 478) the dust fraction was enhanced well above that seen in normal nebulae. It was never necessary to relax either the black-body or the spherical nebula assumptions. This condition, though, should not be confused with any demonstration that the central stars are black-bodies, or that the nebulae are spherical.

The procedure used to iterate toward a solution went roughly as follows. The nebula was first initialized to a set of abundances typical of a Galactic PNe, and to a radius large enough (usually about 0.3 pc) so that the nebula was thick to all ionizing radiation. (To compute this latter condition, we used the [S II] $\lambda\lambda$6717, 6731 density measurement when it was available, otherwise we assumed $N_e = 4,000$ cm^{-3}.) The central star temperature was then varied until the helium

line ratios were approximately correct. For the three PNe where the helium lines were not reliably detected (CJFN 75, 455, and 470), the central star temperatures were constrained by the strength of λ5007 and the upper limits to the helium lines. The central star luminosity was adjusted to yield an approximately correct value for the absolute λ5007 flux. If necessary, the nebula radius was then reduced to lower the line fluxes of the low ionization species (e.g., [O II], [N II], [S II]), and a first adjustment was made to the abundances in order to improve the predicted line ratios.

At this point, secondary adjustments were made to the central star temperature and luminosity, the nebula radius and density, and to the abundances. In some cases, the amount of grains in the nebula was modified as well, in order to achieve a better match with the helium and oxygen lines. Finally, for a few objects, it became necessary to alter the abundances of elements for which no lines were available. The most important of these elements is carbon, whose presence can have a significant effect on the overall cooling efficiency of the nebula. By adjusting the amount of nebular carbon (while keeping it reasonably consistent with the metallicity defined by the other elements), we were able to fine-tune the nebula's electron temperature and improve the corresponding line ratios.

Generally, our nebular modeling approached convergence after 10-20 iterations, although, for a few of the best observed objects, another 20 iterations were needed to achieve a good match to all the line ratios[3]. Table 3 summarizes the parameters describing the 15 nebulae. Included in the table are the derived values for the nebula's electron density, temperature, and radius, the central star's effective temperature and luminosity, and abundance values for helium, oxygen, nitrogen, neon, sulfur, and argon. Because of its importance to the nebular modeling, the assumed carbon abundance is also reported, although no lines of carbon were directly observed. The electron temperatures and densities are volume-averaged quantities.

The central star mass also is included in Table 3. These masses have been computed by interpolating the central star's location in the HR diagram onto the grid of hydrogen-burning evolutionary tracks of Blöcker (1995) and Schönberner (1983). Thus the mass estimates carry the additional uncertainty associated with the applicability of these stellar evolutionary models. In particular, if any of the PNe considered in this survey are helium burners, then their derived mass estimates may be significantly in error.

3.2. Accuracy of the models

In nearly every case, our models were able to reproduce all the observed line ratios to within $\sim$0.02 of the measured value (see Table 2). This is well within the estimated measuring errors of $\sim$ 5% (systematic) plus $>$ 3% (random). For weak lines ($<$ 20% of I(Hβ)) in well-observed objects,

[3]When a doublet is present, such as the $\lambda\lambda$4959, 5007 lines of [O III], the model is forced to match the brighter line of the pair.

the random errors are typically $< 20\%$. Obviously, for fainter objects, the errors are worse.

In the two cases where a multizone density model was required, single zone models yielded abundance values that differed by < 0.3 dex (usually < 0.1 dex). Abundance uncertainties of this magnitude, though, are large. Generally, when the data quality is good to excellent, our abundance measurements are constrained to < 0.1 dex. This is especially true for oxygen, neon, and helium where, typically, the models are constrained to ~ 0.04 dex ($\sim 1\sigma$). Nitrogen and sulfur abundances are more uncertain since these elements have only one visible ion, whose contribution is dependent on the geometry of the nebula. (Although the [O II] λ3727 to [O III] λ5007 ratio does provide an independent measure of this geometry, this constraint is only applicable under the assumption of sphericity.) We estimate that our N/H and S/H are accurate to ~ 0.3 dex. Argon is modeled with good stability, but depends strongly on an accurate measurement of the [Ar III] λ7135 line. Because this feature is generally not well observed, our Ar/H values also are uncertain at ~ 0.3 dex.

With respect to the central star properties, the stellar temperatures are generally constrained to within $\sim 5,000$ K when the He I and He II lines are measured with good accuracy (6 PNe), to $\sim 10,000$ K when only He I is measured well (4 PNe), and to $\sim 20,000$ K otherwise. Similarly, the stellar luminosities are constrained by the [O III] λ5007 fluxes, which are well-determined from photometric observations. Second order factors include the correction for extinction, the adopted fraction of dust in the nebula, and the derived optical thickness to ionizing photons (which comes from the ratio of [O II] λ3727 to [O III] λ5007). Based on our experiments with near-acceptable models, these effects generally introduce an uncertainty of ~ 0.1 dex on the central star luminosity, although the luminosities for PNe with low quality spectra may be in error by up to 0.3 dex.

Since nearly all of the bright PNe considered in this paper are on the horizontal portion of their evolutionary tracks, the central star masses are not significantly affected by errors in temperature. Luminosity errors, however, do propagate into the mass determinations. For typical central stars with $M \sim 0.6$ $M_\odot$, the error in mass is always < 0.07 $M_\odot$, and usually less than ~ 0.02 $M_\odot$.

In the next section, we discuss another aspect of the accuracy of the models.

3.3. Uniqueness of the models

Several authors (Jacoby et al. 1997; van Hoof & Van de Steene 1997) have described attempts to probe the robustness and uniqueness of PN photoionization models. The results are encouraging, but unless there are many emission-lines from many different ions, some level of uncertainty always remains.

For two nebulae having high central star masses (CJFN 27 and CJFN 1), we attempted to derive models with core masses more in line with the other nebulae. These attempts were not

successful; in fact, the masses could not be changed by more than ~ 0.06 $M_\odot$ from the initial converged value. Our models for these objects may therefore be unique.

For the two nebulae requiring multizone density models, we pursued single zone models until it became apparent that such a model would never succeed. Hence, for these objects, single zone models were ruled out. Unfortunately, with the added flexibility provided by a less constrained density distribution, the results for these models may be less secure than those of the remaining nebulae.

Observations of the nebula CJFN 27 were matched with a very high density nebula ($N_e = 89{,}000$ cm^{-3}). To check this, we attempted to model the nebula with a lower, more typical density ($N_e = 9500$ cm^{-3}). This model succeeded in meeting the observational constraints, but in order to maintain a high electron temperature, the carbon abundance had to be reduced by a factor of four, and the dust component had to be increased to 2.4 $\times$ the typical PN fraction. This alternative model also demonstrated marginal stability in the sense that a small change in *any* parameter rapidly drove the solution away from many of the observational requirements. More importantly, while the elemental abundances in the alternate model did change, the worst case changes were only +0.26 dex (for nitrogen) and −0.21 dex (for oxygen).

In addition to these experiments, we pursued one additional test of uniqueness. We attempted to build a model of the reasonably well-observed PN FJCHP 51 with an oxygen abundance 0.3 dex lower than the nominal value, but with no constraints on the strength of the nebula's [O III] λ4363 line. In other words, we simulated the case where this weak, but important, line is lost in the noise. The test failed in the sense that we were not able to create a successful model in which O/H was more than 0.16 dex below normal. Moreover, in order to achieve even this modest level of reduction, the nebula's carbon abundance had to be significantly (and perhaps unrealistically) lowered by 0.9 dex to force a high electron temperature; under these conditions, the [O III] λ4363 line would be 2σ stronger than that observed. From this, we conclude that the maximum deviation in derived oxygen abundance is within the range of the observational errors.

A full investigation into the uniqueness of photoionization modeling is beyond the scope of this paper. Our experience, though, indicates that it is difficult enough to get *any* model to converge to the appropriate line ratios, let alone to devise successful models with vastly different properties.

3.4. The Balmer decrement

During the extinction and reddening correction phase of the reductions, we adopted a standard value of 2.85 for the Balmer decrement ratio of $I(\mathrm{H}\alpha)/I(\mathrm{H}\beta)$. This, however, is a simplification: the true Balmer decrement can range between 2.7 and 3.1, depending on plasma conditions (cf. Ferguson & Ferland 1997; Osterbrock 1989; Ferland et al. 1998). Thus, to be fully self-consistent, we should have revised our extinction estimates based on the derived values for the

electron temperatures and densities and then recomputed our nebular models. This iteration was not performed. For 11 of the 15 PN considered here, the derived ratio for the Balmer decrement was within 1% of the adopted value, and thus the additional iteration was not needed. For the remaining PNe, $I(\mathrm{H}\alpha)/I(\mathrm{H}\beta)$ ranged from 2.76 to 3.06, or ±4%. Since the systematic errors in the line measurements (and uncertainties in the physics of the hydrogen atom) are comparable to, or worse than, this extreme range, we decided that the small error introduced by this effect was acceptable.

3.5. Comments on the nebulae

CJFN 1: [37″ from the nucleus] Although this PN is close to the nucleus, it is very luminous: only 0.5 mag down the PNLF. Consequently, the spectrum has a reasonably high signal-to-noise. Our models demonstrate that this nebula is almost completely optically thick, with a radius that is 97% of the optically thick value. A very high central star temperature is required to meet the strong He II line strength.

We note that RSM also observed this object, though with lower signal-to-noise. They report similar line ratios, at least for those lines that they were able to measure. Whatever differences exist can be attributed to the somewhat lower quality of their spectrum.

CJFN 9: [8″ from the nucleus] This object is very close to the nucleus of M31 and located on top of significant diffuse emission. The combination of a bright stellar background and bright emission from the local interstellar medium rendered this spectrum unusable (i.e., the PN Balmer lines could not be measured). No results are presented for this object.

CJFN 23: [68″ from the nucleus] There are no low excitation lines visible in this PN, but this may be due to the poor subtraction of M31's diffuse emission. Without the low ionization species, there is no way to constrain the ionization structure of the nebula with confidence. The red region of the spectrum suggests that the sky subtraction went well and that the object is a high excitation nebula with very weak lines of [N II] and [S II]. The blue [O II] lines, however, are over-subtracted, but the implications of this are difficult to evaluate because of the instrumental defocussing. In order to model the upper limits on the [N II] and [S II] lines (~ 0.2 of $I(\mathrm{H}\beta)$), a nebula radius of 0.061 pc is required, which is 90% of the optically thick value.

Alternatively, N/H and S/H could be reduced by making the nebula more optically thick and enlarging its radius. If the nebula is made less optically thick, N/H and S/H can be increased substantially. However, in this case, O/H also would have to be increased to meet the nebular flux constraint.

This PN also was observed by RSM; their line ratios agree approximately with ours, but neither data set has a high signal-to-noise ratio.

CJFN 27: [152″ from the nucleus] This PN spectrum is excellent, as might be expected from

a very luminous PN (0.6 mag down the PNLF). Yet, the low ionization lines are extremely faint, with the [N II] lines being the only ones measured with confidence. [S II] is marginally present, but the ratio of $I(\lambda6717)/I(\lambda6731)$ is at the low density limit, which is physically unrealistic for a bright PN. Presumably, if the [S II] intensities are correct, they derive from a very tenuous outer region beyond the main body of the nebula. This object also exhibits very strong [O III] $\lambda4363$ emission; this implies a substantial amount of dust, since this helps the nebula attain a high electron temperature. The large number of lines and ionization states observed, coupled with the excellent diagnostic provided by $\lambda4363$, make this one of our best constrained models. Nevertheless, the very high density deduced for CJFN 27 suggests that an alternative model might be more likely. Unfortunately, our attempts to devise a low density model for this object were only marginally successful (see §3.3). The nebula is optically thick.

CJFN 29: [132″ from the nucleus] Because the [S II] line ratio is at the low density limit, this planetary must contain a significant amount of material at low density. However, the high [O III] flux of the object requires a much higher density; otherwise, in order to produce this flux, the nebula would have to be extremely large and massive. This discrepancy drove us to consider a two-zone density structure for this object.

During the modeling process, we noted that the observed [S II] ratio $I(\lambda6717)/I(\lambda6731) = 1.76$, which suggests a density close to zero. Since this is unphysical, it implies that there is an error of at least $\sim$ 25% in our measurement of these weak lines; presumably, this is due to the poor subtraction of the diffuse ISM present in M31's bulge. To deal with this problem, the density of the model's outer zone (which starts at a radius of 0.054 pc and terminates at 0.462 pc, or 81% of the optically thick radius) was arbitrarily set to a density of 280 cm^{-3}. This forced the sense of the [S II] lines to agree with the observations (i.e., to guarantee that $I(\lambda6717) > I(\lambda6731)$, as seen even in the raw data). The models were then required to match only the brighter of the [S II] lines, while the weaker line floated to a value indicative of the adopted density in the outer zone. Meanwhile, the density of the inner zone was arbitrarily set to 7000 cm^{-3}.

We note that the high value for [O III] $\lambda4363$ presented a minor problem for the models. To offset the very high abundances derived for the object, dust was needed at 90% of the nominal value for PNe. Another oddity is that due to its high abundance ([S/H] = +0.5), cooling via sulfur appears to be very important for this object. On the other hand, this result may be an artifact of the weak sulfur lines and difficult background subtraction.

A single-zone model was also attempted with limited success. For this model, we left the [S II] line ratio unconstrained but matched the total [S II] flux of the object. The result was that none of the abundances changed by more than $\sim$ 15% (0.06 dex) except for nitrogen, which decreased by 0.2 dex. The central star luminosity, however, dropped by 35% since the single zone nebula was more optically thick than the two-zone model.

This nebula is unusual in yet one more way. It is the best observed object in common with RSM, but a major discrepancy exists for the relative strength of [O III] $\lambda5007$. Our value of

14.8 × $I(\mathrm{H}\beta)$ is significantly different than the value that they report (22.2 × $I(\mathrm{H}\beta)$). We and RSM have attempted to resolve this disagreement but have not identified any problems in either of our data sets. We expect our observations to be accurate to $\sim$ 3%. The discrepancy is more mysterious when we consider that the line ratios for two fainter PNe, CJFN 1 and CJFN 23, are in reasonable agreement. One possibility is that CJFN 29 is variable on a short timescale, though we note that the RSM data were taken only 13 months before our observations. In support of this speculation, we do see very good agreement in the derived elemental abundances (Δ [O/H] = 0.04).

CJFN 33: [219″ from the nucleus] The spectrum for this PN is of moderate quality, but no low ionization lines are present. The radius was set to the maximum that did not produce [O II] λ3727 above the observed limit of $\sim$ 0.25 of $I(\mathrm{H}\beta)$. Beyond the UV, most lines as faint as 10% of $I(\mathrm{H}\beta)$ are well measured; the lone exception is He I λ5876, since the velocity of CJFN 33 places the line in the Na I sky feature. Perhaps this is why the derived helium abundance is abnormally low ($N(\mathrm{He})/N(\mathrm{H}) = 0.05$). With $I(\lambda5876) = 0.06\, I(\mathrm{H}\beta)$, this low abundance is inevitable and is independent of any modeling ambiguities. The model is optically thin, with the outer radius at 83% of the optically thick value.

CJFN 75: [78″ from the nucleus] Only the He I line (λ5876) presented a problem in developing a model for this nebula. The measured value of 0.76 of $I(\mathrm{H}\beta)$, though, is very likely to be an artifact of poor background subtraction. The helium abundance was arbitrarily chosen to be 0.148 which is a high value, but not unusually so. The strength of the [O II] lines sets the outer radius to be at 97% of the optically thick value. However, other than the usual requirement for absolute nebular flux, the model is not tightly constrained. Still, we believe the O/H and Ne/H abundances are valid.

CJFN 125: [250″ from the nucleus] Although this bulge PN is relatively far from M31's nucleus, it is intrinsically faint (1.6 mags down the PNLF) and thus, its spectrum is quite noisy. The lines of [O III] λ4363 and [S II] $\lambda\lambda$6717, 6731 were not detected, although lines as faint as 10% of $I(\mathrm{H}\beta)$ are measurable. Given the limited number of lines, a viable model with no dust was found easily. The model is optically thin, with the outer radius at 83% of the optically thick value.

CJFN 177: [206″ from the nucleus] Despite being 1.8 mags down the PNLF, the spectrum of this nebula is very good, and it displays a relatively rich variety of ionization states. Thus, the object can be modeled with enough constraints to delimit abundances fairly well. Lines as faint as 5% of $I(\mathrm{H}\beta)$ are measurable; [O III] λ4363 may have been detected at 2% of $I(\mathrm{H}\beta)$. The model fits all lines (including the limit on λ4363) with a nearly optically thick nebula: the derived outer radius is 98% of the fully optically thick value.

CJFN 179: [234″ from the nucleus] This PN is intrinsically faint, 2.2 mag down the PNLF. Furthermore, it falls on a region of diffuse emission, leading to complications in background subtraction. Lines as faint as 12% of $I(\mathrm{H}\beta)$ are measurable, but the important diagnostic lines are not seen. Given the limited number of lines, a viable model with no dust was found easily. The

model is optically thin, with the outer radius at 81% of the optically thick value.

CJFN 455: [137″ from the nucleus] This PN is very faint and close to the nucleus. It suffers more than any other from background subtraction errors, as evidenced by the negative (i.e., over-subtracted) lines of [O II], [N II], and [S II]. Since the ionization structure could not be derived from the very limited number of line ratios, our model was defined to have a radius at 90% of the optically thick radius, a number typical of many of the M31 PNe. With only lines of [O III] and [Ne III] measurable, this nebula model is very poorly constrained. However, the [O III] luminosity serves to set the luminosity of the central star which, in combination with any likely temperature, allows an estimation of the central star mass.

CJFN 470: [101″ from the nucleus] This PN has the faintest apparent m_{5007} of the sample, 3.0 mag down the PNLF, and it has a relatively low excitation. Due to its faintness, few lines are measured well, and the background subtraction and contamination errors from the diffuse ISM of M31's bulge are significant. Abundances and stellar parameters are indicative, but not accurate. Since the error in $I(\mathrm{H}\beta)$ alone is $\sim$ 20%, no line ratios are more accurate that this; nevertheless, a model with the standard 2% error was devised. The model required a central low density (140 cm^{-3}) region extending out to 0.50 pc; beyond that and to a radius of 0.62 pc, a density enhancement $\mathrm{N}_e \sim 250$ cm^{-3} is required. Although there are very few constraints to the model, two could not be matched. First, the He I line at λ5876 is so strong that it must be an artifact; the spectrum is very noisy in this region and the apparent line is blended with sky emission. Second, the weaker [S II] line (λ6731) could not be matched within the usual tolerance (0.02 of $I(\mathrm{H}\beta)$), but was reproduced at a strength of 1.66 $I(\mathrm{H}\beta)$, 13% lower than observed. Given the large diameter of this nebula (1.24 pc, or 0.″33), the object should be easily resolvable with the *Hubble Space Telescope* if the model is correct.

CJFN 478: [137″ from the nucleus] This nebula presented a number of problems in the modeling. First, the [O III] λ4363 line is measured to be moderately strong at 0.042 $\times$ $I(\lambda5007)$: this indicates a high electron temperature, $T_e = 22,000$ K. However, to attain this temperature, the carbon abundance (and its cooling contribution) must be decreased significantly, and the amount of dust grains must be increased to five times the normal PN dust-to-gas ratio. The high dust factor serves two roles: it reduces the nebular cooling by depleting the metals onto grains, and it provides an additional heating source via photoelectric emission (Borkowski & Harrington 1991). Unfortunately, the addition of so much dust also reduces the emitted luminosity of the nebula, forcing the central star to be intrinsically more luminous and massive ($M > 0.9$ $\mathrm{M}_\odot$). Given the halo-like abundances of this nebula, this seems unlikely. The alternative is to suppose that the flux from [O III] λ4363 has been overestimated; since the signal-to-noise of the line is not high (the line is only measurable to $\sim$ 30% accuracy), this possibility is quite viable. On the other hand, we also have a marginal detection of the [N II] λ5755 line, which provides additional evidence for a high electron temperature.

Because of this confusion, the results presented in Table 3 represent those of a compromise

model that trades off between a high dust content and a high central star luminosity. In the model, the dust is enhanced by a factor of 3, the central star mass is $\sim 0.88 M_{\odot}$, and the strength of [O III] λ4363 is assumed to be 30% smaller than actually observed. This model has a radius of 0.36 pc, only 5% short of the optically thick value.

A similar uncertainty arises when we consider the strength of [O II] λ3727. The high ratio of [O II] λ3727 to Hβ (1.05) is easily reproduced with a two-zone density model. In fact, the compromise model yields $I(\lambda 3727) = 1.12$; in the model, the inner nebula (radius < 0.018 pc) has a moderately high density (11,000 cm^{-3}), while the outer region (extending to a radius of 0.36 pc) has $N_e \sim 460$ cm^{-3}. Again, however, the [O II] line suffers from an added uncertainty associated with the contribution of irregularly distributed diffuse emission in M31's bulge. Moreover, in this part of the spectrum, instrumental factors (low sensitivity, defocus of the spectrum in the camera) combine to lower the signal-to-noise of the measurement. Consequently, a single zone model does as well as the two zone model if the strength of the [O II] line is allowed to drop by almost a factor of two, to 0.65 I(Hβ). This degree of error is unlikely, so we adopt the compromise dual zone model. The differences in the abundance determinations between the single and dual zone models are always < 0.15 dex.

FJCHP 51: This PN and the other two outer PNe were far easier to observe than any of the bulge objects because of the much lower background levels. Consequently, the models for these three objects have much better constraints than those for their bulge counterparts. For example, both the [O III] λ4363 and [N II] λ5755 temperature sensitive lines, as well as the density sensitive lines of [S II], were measured in this nebula. An excellent match to the observed line ratios was obtained with a radius at 93% of the optically thick value.

FJCHP 57: This intrinsically luminous PN exhibits relatively low abundances. The spectrum is very good and has the unique property that features from the central star are visible. The Wolf-Rayet signatures at λ4650 from (N III, C III, and C IV) and λ5806 (from C IV) are seen easily. The relative strengths of these lines, plus the absence of other Wolf-Rayet indicators, suggest that this central star is approximately a WC 6 class object (van der Hucht et al. 1981). The temperature calibration of Tylenda, Acker, & Stenholm (1993) then gives $T_{eff} \sim 50,000$ K, in excellent agreement with the temperature of 58,000 K needed by the photoionization model to match the observed strength of the helium line at λ5876. The nebula is nearly optically thick, with a radius at 98% of the optically thick value.

FJCHP 58: This is a high excitation PN with no evidence for lines of [O II], [N II], or [S II]. This lack of emission is significant, since the spectrum has a fairly high signal-to-noise, and non-UV lines as weak as 4% of Hβ should be seen. (For [O II], the limit for detection is closer to 20% of Hβ.) The geometry was defined to meet these limits, leading to a radius that is 86% of the optically thick value. The relatively low luminosity of the nebula is responsible for the low central star luminosity and mass.

4. Results

4.1. Abundance comparison with ICF method

In the 8 cases where plasma diagnostics allow a direct comparison between nebular models and measurements based on ionization correction factors or "ICFs" (e.g., Alexander & Balick 1997), we generally find good agreement in the abundances. The summary of the differences between the CLOUDY and the ICF abundances (as formulated by Alexander & Balick 1997) is given in Table 3. On average, the photoionization method yields slightly higher abundances, typically 20% (0.08 dex). Moreover, for the worst case nebula, CJFN 27, if the alternative low density model is adopted, the agreement with the photoionization models is improved, but CLOUDY still yields higher abundances by 15% (0.06 dex). Since nebula CJFN 27 is responsible for the most extreme difference between the two abundance techniques, the latter estimate is more typical of the sample as a whole.

The abundance differences between the CLOUDY photoionization results and the values derived from the ICF method arise from two primary parameters: T_e and N_e. First, the model's estimate of T_e assumes a limited uncertainty in λ4363; in contrast, the ICF method accepts the observed strength of λ4363 as exact. Thus, within the observational uncertainties, the two methods will yield the same abundances if T_e is the dominant source of difference. Second, the density suggested by the [S II] lines is very uncertain, both because these lines are usually weak in high-excitation planetaries, and because the low-excitation diffuse emission in M31's bulge complicates the background subtraction. (Indeed, as described above, the implied [S II] densities can occasionally be unphysical.) Because the ICF method assumes that the [S II] ratios are exact, errors in their measurements will affect ICF abundances more than model derived values.

Based on the above arguments, we conclude that even when line ratios are available for ICF measurements, there still is a small advantage in accuracy obtained by deriving abundances of extragalactic PNe via photoionization models. Alexander & Balick (1997) also concluded that the ICF methods generally are adequate, but could suffer additional inaccuracies under certain conditions.

4.2. Abundance comparison with SRM

We observed 3 PNe in common with the sample of SRM (CJFN 1, 23, and 29). Given that the observations, reductions, and analysis are completely independent and utilize very different approaches, these objects provide a valuable external test of the errors in the abundances. Immediately obvious is the fact that the SRM abundances for helium in all three objects are unrealististically low, typically He/H ~ 0.015. Our values are closer to those observed in Galactic and Magellanic Cloud PNe. For oxygen, however, the agreement is excellent: the logarithmic difference in the two measurements is ΔO/H $= -0.013 \pm 0.05$ (ours minus SRM). The results for

neon are mixed, with ΔNe/H = 0.00 $\pm$ 0.18. Although there is no systematic offset between the abundance determinations, the dispersion between the two neon measurements is large.

The fact that the neon measurements exhibit a large amount of scatter should not be too surprising. The abundance of neon is based on a single, relatively weak line of [Ne III] at λ3869. Thus, with only one ionization state available, abundance measurements carry a larger than normal uncertainty, especially for ICF-based values. In addition, the [Ne III] line lies well into the UV, where system sensitivities are poor and where atmospheric dispersion effects in uncompensated observations have the greatest impact. (Our observations were made using the atmospheric dispersion corrector built into the 4-m telescope.) Nevertheless, it is comforting to see that there appears to be no serious zero-point errors between the measurements.

4.3. Abundance correlations

Further confidence in the derived abundances of O and Ne is provided by their very tight correlation (first noted by Henry 1989). This is displayed in Figure 3. It is clear from the figure that our PNe sample exhibits a wide range of oxygen abundances from 0.05 solar to marginally super-solar with a clump of objects near O/H $\sim$ 8.35.

Also plotted in Figure 3 are the abundances measured by SRM. Their PNe follow exactly the same locus as the 15 objects presented here, but exhibit higher median abundances. (This is due to a selection effect in luminosity; see §4.4.1.) There are, however, 2 PNe in our sample that lie off the main locus of points – FJCHP 57 and CJFN 455. FJCHP 57 is a high velocity planetary that has generally low abundances reminiscent of halo PNe in the Milky Way. Henry (1989) has found that Galactic halo planetaries can deviate from the main locus in the O–Ne correlation. If FJCHP 57 is really a halo PN in M31, it is projected on a disk field and is therefore a fortunate find. CJFN 455, on the other hand, is a very faint object with a marginal measurement for neon. Thus, it is not significant that it falls off the O–Ne relation.

In Figure 4, we show the correlation between N/O and N/H. Even with the limited data, it is clear that the trend seen by Henry (1990), and shown by the dashed line, is followed by the M31 PNe. The slope of the trend is 0.96, which is close enough to unity to suggest that variations in N/O are due almost entirely to variations in N, independent of O. That is, nitrogen is not being manufactured at the expense of oxygen. This conclusion is supported by the absent, or possibly weak, anti-correlation between N/O and O/H (Figure 5). A similar weak anti-correlation has been reported by others for Type I PNe (see Henry 1990 and references therein), but this was not seen in the large sample of Kingsburgh & Barlow (1994).

The correlation seen in Figure 4, though, could be due entirely to large observational errors in N/H, since those would affect N/O similarly. This explanation, however, would also have to apply to Henry's sample unless one accepts a coincidence of nature in which our (accidental) correlation matches Henry's real one.

Figure 5 presents a variety of relationships (or lack thereof) between N/O and He/H, O/H, extinction, m_{5007}, and core mass. Four of the objects have log (N/O) > -0.3 and He/H > 0.125; according to the criteria of Peimbert & Torres-Peimbert (1983), these are Type I planetaries. This is somewhat surprising: in the Galaxy, Type I PNe are presumed to derive from younger, more massive progenitors, yet three of these putative Type I PNe are located in M31's bulge. Moreover, if, in fact, our Type I PNe do arise from massive progenitors, we might expect the high N/O objects to be brighter than their low N/O counterparts, since their central stars would be more luminous and more massive (cf. Méndez et al. 1993). The anti-correlation between N/O and m_{5007} (Figure 5), a consequence of added nitrogen competing with oxygen to cool the nebula (Jacoby 1996), shows that the opposite is true. In fact, the lack of correlation between N/O and core mass argues that although our PNe with high N/O may have abundances typical of Type I PNe, their central stars come from an older, less massive population. Probably some, or all, of these objects are not true Type I PNe, but exhibit high N/O and He/H because their progenitors were enriched (see also SRM). Curiously, our Type I candidates tend to be among the least dusty PNe in our sample. But this could be a selection effect: a highly extincted object would not have been detected in the CJFN survey.

No other clear trends between abundances are seen. There may be a weak positive correlation between Ar/H and O/H, but the errors in the argon line ratios are large enough to render any such trend suspect.

4.4. Other correlations

4.4.1. abundance and luminosity

Given that the strength of the [O III] lines is proportional to the number of oxygen atoms, one might expect that, all things being equal, an oxygen-rich PN would be more luminous in λ5007 than an oxygen-poor object. However, all things are not equal.

With more oxygen (and presumably more of other elements as well), nebular cooling is more efficient. This lowers the nebular electron temperature and decreases the collisional excitation that drives the [O III] lines. As a result, the nebular luminosity in λ5007 is expected to rise roughly as the square root of O/H rather than O/H directly (Jacoby 1989; Dopita et al. 1992). The effects of metallicity are then complicated further by the PN progenitor's evolution prior to its departure from the AGB. High metallicity stars are expected to have high mass loss rates (Mowlavi et al. 1998; Greggio & Renzini 1990) and, consequently, should form lower mass central stars than their low metallicity counterparts. As a result, the luminosity of the central star (and the nebula) should be lower if the progenitor is metal-rich. But, as noted just above, nebular cooling is somewhat more efficient when there are large numbers of atoms. The two PN components, the nebula and the central star, therefore behave in offsetting ways. A detailed analysis shows that the peak in the [O III] luminosity is expected for PNe with metallicities between the LMC and solar (Dopita,

Jacoby, & Vassiliadis 1992; Ciardullo & Jacoby 1992).

Figure 6 shows how the apparent brightnesses of the M31 PNe vary with O/H and Ne/H. We include SRM objects in our plot because their sample includes more of the brightest PNe than are present in our dataset. (We intentionally selected targets to extend over a wide range of luminosity in order to probe luminosity-dependent abundance patterns.) The observations demonstrate that the brightest PNe are nearly independent of O/H. That is, the upper envelope of magnitudes is flat to within ± 0.1 mags over a range of 1 dex in O/H. Thus, we support the conclusion of Kennicutt et al. (1998), who found that the differences between PNLF and Cepheid distances are nearly independent of metallicity. These data, coupled with the correlation between maximum [O III] flux and O/H found at lower metallicities (Richer, Mc Call, & Arimoto 1997), also confirm the conclusion of Ciardullo & Jacoby (1992), that the sensitivity of the PNLF cutoff to metallicity is only important for populations more metal poor than the LMC.

On the other hand, Figure 6 also demonstrates that there is a slight tendency for fainter PNe to be drawn from a lower metallicity population. If real, then the shape of the PNLF could be metallicity-dependent even if the maximum [O III] luminosities remain insensitive to abundance. We suspect, though, that this trend is an artifact of a selection effect or an analysis bias because there is no physical rationale why metal-rich PNe should not be faint as well as bright. Most likely, an unbiased distribution in O/H drops off steeply towards high O/H (as it does in our Galaxy). Because the SRM sample is larger than ours, it will include more high O/H PNe than ours, and since it also draws from a brighter sample than ours, an apparent deficit of faint, high O/H PNe may be the result.

4.4.2. luminosity and central star mass

Figure 7 illustrates the absolute magnitude, M_{5007}, of the PNe as a function of central star mass, corrected for extinction and distance. We see a clear trend of the sort one expects – that is, more massive central stars produce more luminous planetaries. At face value, this suggests that young populations should produce luminous PNe (at λ5007) which would make the cutoff in the planetary nebula luminosity function depend on population age. Yet, when we look at Figure 8, which shows the apparent PN magnitudes, m_{5007}, as a function of central star mass, the trend is much less evident. This suggests that the PNLF has, at best, only a mild dependence on stellar age. Quantitatively speaking, if we ignore the stars with core masses >0.8 $M_\odot$, then there is a 99.93% probability that M_{5007} is correlated with core mass (i.e., a 3.4σ effect) but only a 92.72% probability that m_{5007} is correlated (a 1.8σ confidence level). This behavior can be understood by examining the only parameter that can effect a difference between Figures 7 and 8 – extinction.

4.4.3. extinction and central star mass

Figure 9 shows that a correlation exists between extinction to the individual M31 PNe and their central star masses. It operates in exactly the manner expected – lower core mass objects have less extinction. Thus, the lower central star luminosities of low core mass PNe are partially compensated by also having less extinction to dim their nebulae. A corollary to this observation is that the luminosities will be less constant at other wavelengths since extinction is highly dependent on wavelength. For example, one might expect that, when observed in C III] λ1909, the brightest planetary nebulae will be those with low-mass central stars, since the impact of extinction is greater in the UV.

There is some circularity in the relationship between extinction and central star mass. A positive error in the Balmer decrement can induce an overestimate of the extinction. This error will, in turn, cause the extinction-corrected nebular luminosity to be overestimated, and hence, the luminosity of the central star will be overestimated. Since core mass is derived from a star's position in the HR diagram, an overestimate of central star luminosity leads directly to an overestimate of central star mass. Consequently, errors in the data will introduce a correlation of the type seen here, but at a level about 4–6 times smaller than observed.

Ciardullo & Jacoby (1999) discuss this correlation in detail. A plausible rationale for its existence can be described briefly in the following manner. Large core mass PNe are presumed to derive from relatively massive progenitors. Most of the progenitor's mass is ejected during the AGB phase; consequently, PNe with slightly higher mass central stars have considerably more material in and around their nebulae. Moreover, the timescale for an AGB star to evolve into a planetary nebula is extremely sensitive to mass. Low mass stars evolve to the blue very slowly, giving their circumstellar matter time to disperse, while high mass stars go from the AGB phase to a high-excitation PN quickly, when their ejecta is still close by. As a result, PNe formed from high mass stars will be surrounded by a large, dense dust cloud, while low mass PNe will have less circumstellar dust, and have it at lower density. A correlation between extinction and core-mass is the natural result.

4.5. Abundance summary

The average (by number, not log) and median abundances of nitrogen, oxygen, neon, argon, sulfur, and helium are given in Table 3. (Recall that the values for carbon are not meaningful, except to document the abundances used in the models. That is, they are assumed, rather than calculated.) For comparison, Table 3 also includes the abundance values for the Sun, and average values for PNe in the Milky Way, the LMC, the SMC, the Sagittarius dwarf, and NGC 5128 (Cen A). Also listed are the abundances of the Orion H II region.

The M31 helium abundances are comparable to, or slightly higher than, those in the Milky

Way PNe. On the other hand, the median abundances for the remaining elements are in surprisingly good agreement with the average for the LMC sample given by Clegg (1992). The recent re-analysis of the LMC and SMC PNe by SRM, though, shows 2 significant effects in this regard. First, SRM find that luminous PNe are more metal-rich than low luminosity PNe (see also §5.1.2), which suggests that a direct comparison of abundances is risky unless one compares PNe of similar luminosity. Second, they find that the PNe in their high-luminosity sample have O/H 0.15 dex smaller and N/H $\sim$ 0.35 dex smaller than the values reported by Clegg. Since the SRM high luminosity sample should be more metal-rich than the Clegg PNe, this indicates that analysis methods can play an important role in these comparisons. (We adopted Clegg's values for Table 3 because he presented a single set of abundances that includes neon, sulfur, and argon, whereas SRM present only oxygen and nitrogen).

The similarity of the M31 PN abundances to those of LMC PN is unexpected in light of the high abundances derived from the integrated stellar spectra. We discuss this conundrum below.

5. Discussion

5.1. LMC abundances for a super metal-rich population?

The abundances derived from the integrated light of galaxies generally yield calibrated abundances only for [Fe/H]. While absorption indices such as CN and CO provide limited information about the lighter elements (Burstein 1985), a direct quantitative comparison for light element abundances between the stars and PNe is not possible. Consequently, we will compare [Fe/H] from the stars in M31 to [O/H] from the PNe.

The primary question raised by Table 3 is the following: given that the integrated properties of the bulge starlight in M31 exhibit clear signatures of high metallicity, with [Fe/H] $\sim$ +0.25 (see §1), why do the PNe in M31 appear to be so similar to the LMC PNe? After all, the LMC is generally considered to be dominated by stars with [Fe/H] $\sim$ −0.4 (Olszewski, Suntzeff, & Mateo 1996) and surveys in this galaxy demonstrate that the PNe have similarly low abundances (Dopita & Meatheringham 1991a; Dopita & Meatheringham 1991b; Clegg 1992; Dopita et al. 1997). The same can be said for the Galactic bulge: the mean metallicity of the stars is [Fe/H] $\sim$ −0.25 (McWilliam & Rich 1994) while the Galactic bulge PNe have [O/H] $\sim$ −0.3 (Ratag et al. 1997). But in M31, there is a clear misalignment of >0.5 dex between the expected and observed abundance patterns. We consider several explanations for this discordance.

5.1.1. Metal-rich stars cannot make bright PNe

We must keep in mind that we are only surveying the brightest PNe in M31's bulge. Thus, the entire issue can be side-stepped if metal-rich stars do not make bright PNe. Although far from

certain, if mass loss prior to the PN phase increases with metallicity (Mowlavi et al. 1998; Greggio & Renzini 1990), then at some high level of metallicity, only very low mass remnant stars will be produced. These will result in faint or possibly "invisible" PNe. Moreover, if the central star falls below a critical mass (~ 0.55 $M_\odot$), it may become a "lazy central star" (Schönberner 1983), which will evolve too slowly to ionize its ejecta. This effect is likely to occur in an old, low mass population (Jacoby et al. 1997). Thus, it is possible that a large fraction of M31's high-metallicity bulge stars won't produce bright planetaries.

There is supporting evidence for this scenario – CJFN estimated that the PN production rate of M31's bulge is about half that expected from the total stellar death rate (Ciardullo 1995). Similarly, despite the large range of metallicity observed for Milky Way bulge stars, the survey by Ratag et al. (1997) found only one PN out of 103 where O/H exceeds solar by more than the error bar.

Figure 10 shows the distribution function for O/H in the M31 and Milky Way bulges. The total M31 sample (ours plus SRM's) is statistically identical to that of the Milky Way: a Kolmogorov-Smirnov test shows that the two distributions are different only at the 42% confidence level ($0.55\ \sigma$) – that is, they cannot be distinguished with any confidence. Moreover, both distributions contain very few super-solar PNe, especially when one considers that the uncertainty in the oxygen abundances is typically 0.1 dex or greater for the M31 sample and ~ 0.3 dex for the Galactic bulge sample.

Another comparison of PN and stellar abundances measurements can be attempted in M32. Freedman's (1989) distribution of stellar metallicity, [M/H], shown in her Figure 8, is similar to the PN O/H distribution seen here in Figure 10. Based on various color indicators, Freedman derives a mean metallicity for M32 of [M/H] ~ -0.5. This compares to the [O/H] value of -0.66 obtained by SRM from spectroscopy of 9 PNe. This difference becomes more significant when one considers that solar neighborhood stars with [M/H] ~ -0.5 have [O/H] ~ -0.4, and suggests that the differential in metallicity indicators is -0.26 dex in M32 relative to the Galaxy. Moreover, the colors obtained by Grillmair et al. (1996) for an inner field of M32 ($1 - 2'$ from the nucleus) indicate that that galaxy's [M/H] abundance is significantly higher (-0.25), thus implying an even stronger disagreement with the PN [O/H] measurement.

Therefore, for M31's bulge and possibly M32 as well, the PN abundances appear to be ~ 0.3 dex lower than the mean metallicity of the stars. This seems to indicate that either metal-rich stars do not produce bright PNe or there is a zero-point offset in the two different approaches to deriving metallicities.

5.1.2. There is a selection bias against metal-rich PNe

We have already noted that our sample of PNe was chosen to cover a relatively wide range of [O III] λ5007 luminosity, more-or-less uniformly. Consequently, the 15 PNe studied in this survey

extend more than 2 mags across the PNLF, and nearly 3 mag below the maximum [O III] λ5007 brightness attainable by a planetary. This contrasts with the SRM sample, which is concentrated toward the top magnitude of the PNLF. On average, the SRM sample of PNe have higher abundances than the PNe we observed, with a median O/H of $\sim$ 8.7 and median Ne/H of $\sim$ 7.9 (see Figure 6). In other words, the SRM sample is $\sim$ 0.3 dex more metal-rich than our own; this suggests that interpreting our results as "LMC-like" may be overly simplistic.

The most fundamental conclusion that we can safely state is that there is a considerable spread in the abundance properties in the M31 bulge PNe. Since elements such as oxygen, neon, and argon are not changed significantly within their parent stars prior to ejection of the nebula (van den Hoek & Groenwegen 1997; Forestini & Charbonnel 1997; Aller 1994), a large spread in progenitor abundances is likely. Thus, the stars in the bulge of M31 must have a wide range of properties, and that referring to the "metallicity of the bulge" as a single parameter makes no sense. One must consider the stellar populations problem more generally and refer to each elemental abundance as a distribution function.

Given that there is a spread in the stellar abundances of M31's bulge, it is possible that selection effects operate to favor the observation of low-to-moderate metallicity objects. In fact, one such selection effect has already been discussed; in §4.4.1, we noted that the most favored abundances for bright PNe occurs between the LMC and solar metallicity.

5.1.3. [O/H] and [Ne/H] don't correlate directly with [Fe/H]

For Galactic field stars, [O/Fe] decreases with increasing [Fe/H] (Edvardsson et al. 1993; King 1994; Gratton et al. 1996). At very low metallicities, [O/Fe] $\sim$ +0.5. When [Fe/H] $\sim$ +0.2, though, [O/Fe] has dropped to ~ -0.2, giving [O/H] $\sim$ 0.0. At higher metallicities, one presumes that the trend continues, but data at [Fe/H] $>$ +0.2 is very sparse. If we assume that the bulge of M31 has a similar chemical enrichment history as the nearby field stars, then we should expect to see M31 bulge PNe with [O/H] $\sim$ 0.0 (i.e., O/H $\sim$ 8.9). In fact, we do see several objects in this regime, and perhaps these oxygen-rich PNe derive from iron-rich progenitors while the oxygen-poor PNe truly derive from iron-poor progenitors. Unfortunately, we do not have iron abundances for the PNe, nor do we have oxygen abundances for the stars.

On the other hand, if the PNe studied in our survey come from stars with high [Fe/H], then we are compelled to consider chemical enrichment scenarios that differ from that of the local neighborhood. For example, the bulge stars of M31 could have been created in an environment where the SN II population (a main source of oxygen) was quickly truncated relative to the SN Ia population (a main source of iron). For example, if the bulge of M31 was formed from the accretion of many dwarf galaxies, whose early history was dominated by supernova driven winds, then it is possible that star formation could have been terminated before oxygen was fully enriched. In such a scenario, iron enrichment would come later, as the result of Type Ia supernovae, and an

anomalously low O/Fe would be the result. This model fails in detail, since it predicts a bulge iron abundance similar to that seen in dwarf galaxies (e.g., [Fe/H] < -1; Caldwell et al. 1998), but it does demonstrate how O/Fe might be modified.

WFG considered several solutions to the related, but opposite problem: that of enhanced [Mg/Fe] in the nuclei of galaxies. Since our observations are of M31's bulge, the same mechanisms may operate to increase Mg/Fe in the center of a galaxy and decrease O/Fe further out. For example, the two most plausible processes described in WFG are

1. a gradient in the distribution of stars with $M > 15M_{\odot}$. If few massive stars formed in the bulge of M31, then the descendent Type II SNe would have produced few light elements in the bulge. Conversely, if massive stars were common near the nucleus, then Mg/Fe in this region could have been enhanced.

2. a slower formation time scale for the bulge compared to the nucleus. If the bulge of M31 was built slowly in hierarchical fashion, then there is more time available for Type Ia SNe to enhance iron without drastically affecting oxygen.

Thus, the different results in the two regions could be ascribed to the differing environments; the nucleus is small (enrichment time scales are short) and has a high density (high mass stars may form more easily).

5.1.4. A gradient in [O/H] in the bulge of M31?

Historically, the high values (+0.25) of [Fe/H] in M31 are based on observations taken very close to the nucleus, and may even represent a nuclear population that is very different from the surrounding bulge stars. Our PNe are typically $\sim 150''$ from the nucleus. Davidge (1997) measured the gradients in [Fe/H] for the bulge of M31 out to $60''$, and if we extrapolate his results to a radial distance of $150''$, then we predict that [Fe/H]$\sim$ 0.0. Considering that the PNe also have a line of sight distance from the nucleus that we are ignoring, then a solar composition might be the largest we should expect. Furthermore, King (1994) shows that stars in the solar neighborhood have [O/Fe]~ -0.1 when [Fe/H]$\sim$ 0.0. In the presence of an abundance gradient in M31, we may need to redefine our expectations for the PNe to a median O/H$\sim$ 8.8, or smaller.

Further support for a significant abundance gradient comes from Mould & Kristian (1986), Reitzel, Guhathakurta, & Gould (1998), and Holland, Fahlman, & Richer (1996) who found that stars in the outer spheroid (> 7 kpc) of M31 have [Fe/H]~ -0.6 and that the spread in metallicity is nearly 2 dex. Thus, between the very center of the galaxy and ~ 7 kpc out, the metallicity has dropped off rapidly. The median [O/H] value derived from the PNe is -0.5 to -0.2, depending on the PN sample. At a typical galactocentric distance of 0.5 kpc, this [O/H] is intermediate between the metal-rich and low metallicity stellar populations.

5.2. The halo PNe

Among our 15 PNe, there appear to be two candidates for classification as halo objects. This is somewhat surprising in that, in our Galaxy, less than 1% of the known PNe belong to this group. The most curious halo candidate is CJFN 478, having abundances that are 4 to 18 times lower than solar. The central star mass, however, is deduced to be $0.88M_{\odot}$, and if we adopt the initial mass-final mass relation of Weidemann & Koester (1983), the progenitor mass is derived to be $M \sim 5M_{\odot}$. Clearly, this value is inconsistent with membership in an old halo population.

While the properties of this bulge PN could be explained by invoking a recent star formation episode or capture of a young, low-metallicity satellite system, neither of these ideas has strong supporting evidence. CJFN 478 does have one of the highest velocities among our 15 PNe, with $v = +15$ km s^{-1} observed, or +305 km s^{-1} relative to the systemic velocity of the galaxy. This is almost three times the stellar velocity dispersion in the region (McElroy 1983). Given 12 bulge PNe, one is unlikely to encounter any object having a velocity $> 3\sigma$ from the mean, since the probability of finding one is 0.3%. Thus, statistically, there is some kinematic evidence to believe that this PN might have come from an accretion event. Alternatively, this could be a halo PN with a massive central star formed through a binary coalescence.

The other halo candidate is FJCHP 57, which has abundances 2 – 4 times below solar, except for neon which is highly deficient (40× below solar). As noted in §4.3, FJCHP 57 is peculiar in that it lies well off the oxygen–neon correlation. Furthermore, FJCHP 57 has a velocity ~ 400 km s^{-1} more positive than the other two disk PNe, which are within 70 km s^{-1} of each other. Thus, it is likely that this object comes from a different kinematic population.

Given that we have stumbled on 2 halo PNe out of a sample of 15, one might suspect that the halo component of M31 is very luminous compared to that of the Galaxy. It is premature, though, to comment further on the halo population of M31 until a larger sample of PNe are observed, both for abundances and kinematics.

5.3. Disk vs bulge abundances

Interestingly, if we discount the halo object FJCHP 57, then the two disk PNe, which are at a projected galactocentric radius of 14 kpc, have essentially the same median abundances as the 12 bulge PNe. That is, with the limited sample from this paper, there is no evidence for an abundance gradient between 0.5 kpc from the center of M31, and a region well beyond where the solar circle would fall.

On the other hand, if we mix the SRM PN sample in with ours, then there is a mild gradient in the medians. Since the distribution of abundances in the bulge extends both well above and well below the abundances of the two disk PNe, it is clear that a simple gradient in the median fails to characterize the two samples properly. One needs dozens of PNe, both in the bulge, and at

a variety of galactocentric radii, to define the chemical gradient of M31's stars. Given the number of PNe available for study, such measurements are feasible.

A previous attempt to measure the abundance gradient in M31 from PNe (Jacoby & Ford 1986) also found a small gradient, but that was based on only three PNe. Other methods (HII regions, supernova remnants) identify a mild gradient as well (Dennefeld & Kunth 1981; Blair, Kirshner, & Chevalier 1982).

5.4. Evidence for a merger event?

Our limited sample of 13 bulge PNe shows no evidence for spatially correlated abundances. If we include the additional 25 bulge PNe from SRM (their 28 bulge PNe include 3 of ours), one abundance coincidence emerges. Within a 1 arcmin region (220 pc) containing the PNe CJFN 28, 29, 30, 31, and 80, the average O/H is 8.95 ± 0.11; for comparison, the surrounding PNe typically have O/H $\sim$ 8.35. Thus, over a 10 arcmin field from which the sample of 38 PNe were selected, half of the PNe with O/H $>$ 8.80 are found within 1 arcmin of each other; the remaining high metallicity PNe are distributed fairly randomly across the bulge field (although mostly to the west of the nucleus). Velocities of the 5 PNe comprising the high O/H concentration will provide a critical test of the possibility that these PN are remnants of a merger event. If the kinematics confirm an association among these 5 PNe, then we know from the PN production rate that the accreted object is comparable in luminosity to the M31 dwarf elliptical companions NGC 147 and NGC 185 (CJFN; Ford, Jacoby, & Jenner 1977).

On the other hand, the metallicity–luminosity relationship among galaxies argues that a dwarf elliptical galaxy would not have the high abundance levels exhibited by these 5 PNe. The merger prospect can still be salvaged if the PN grouping derives from the central dense region of a larger galaxy that otherwise has been disrupted and dispersed into the general bulge population. Thus, the possible merger of metal-rich stars is far from settled.

5.5. Future directions

The M31 study presented here, plus that published by SRM, illustrate that PNe provide a direct way to probe elemental abundances, their distributions, and their gradients in old populations. Furthermore Walsh et al. (1998) derived abundances for 5 PNe in the nearby peculiar elliptical galaxy, NGC 5128 (Cen A), demonstrating that 4-m class telescopes can be used to investigate the properties of individual stars in the halos of galaxies four times further than M31. With 8-m class telescopes at excellent sites, one can expect to derive the properties of the old stellar populations in many more elliptical and spiral galaxies. Such observations should completely clarify the ambiguity about the color gradients of galaxies, i.e., whether they are due to age differences or compositional differences.

6. Conclusions

The principal conclusions of this paper are:

1. The very large dispersion in abundances for the bulge PNe of M31 indicates that the stellar population must be highly diverse and that one cannot characterize the bulge with a single metallicity. Instead, it is far more appropriate to refer to the distribution functions of each element.

2. The PNe in the bulge of M31 have abundances that are typically sub-solar. The median abundances could be as low as those in the LMC ([O/H] ~ -0.5), or, if the sample is restricted to only the most luminous objects, the abundances may be 0.3 dex higher than the LMC. Several factors can account for the apparent disparity between this value and the super-solar abundance measured for iron. Among these is the possibility that metal-rich stars fail to produce bright PNe, that PNe with sub-solar abundances are preferentially found in flux-limited samples, and that [O/Fe] drops when [Fe/H] is high. An abundance gradient within M31's bulge may also contribute to the discrepancy. In any case, the metallicity dispersion of the PNe in M31's bulge is significantly larger than that seen in the LMC.

3. The maximum [O III] λ5007 luminosities attained by PNe are highly independent of their oxygen abundances. There is, however, an unexplained trend that the median abundances increase with increasing luminosity.

4. The PN luminosity increases as central star mass increases (i.e., PNe from massive progenitors are brighter), but when apparent magnitudes are measured, this trend is offset by increased extinction.

5. There may be a mild abundance gradient from the bulge of M31 out to the disk field at 14 kpc.

6. There is a clump of 5 spatially coincident high-metallicity PNe about 2.5 arcmin northeast of the nucleus of M31. If they prove to have similar radial velocities, these objects would indicate that a metal-rich satellite galaxy has recently merged with the bulge of M31.

7. We tentatively identify 2 halo PNe in our sample of 15. This ratio is much higher than seen in the Galaxy, and if correct, is either fortuitous or indicative of a much larger halo population in M31 than in the Galaxy.

Discussions with Gary Ferland, Paul Harding, Rob Kennicutt, Heather Morrison, and Michael Richer proved invaluable at various stages of this study. Comments provided by Grazyna Stasińska and Lawrence Aller on an earlier version of this paper helped clarify the presentation immensely. GHJ wishes to thank Dr. Peter Strittmatter for generously providing all office needs during a

sabbatical stay at the University of Arizona where most of this paper was written. RC wishes to thank Dr. Sidney Wolff for providing office facilities at NOAO during a sabbatical stay during part of the development of this paper. RC was partially supported by NSF grant 92-57833 and NASA grant NAG 5-3403.

REFERENCES

Alexander, J., & Balick, B. 1997, AJ, 114, 713

Aller, L. H. 1994, ApJ, 432, 427

Bica, E., Alloin, D., & Schmidt, A. A. 1990, A&A, 228, 23

Blair, W. P., Kirshner, R. P., & Chevalier, R. A. 1981, ApJ, 247, 879

Blöcker, T. 1995, A&A, 299, 755

Borkowski, K. J., & Harrington, J. P. 1991, ApJ, 379, 168

Burstein, D. 1985, PASP, 97, 89

Caldwell, N., Armandroff, T. E., Da Costa, G. S., & Seitzer, P. 1998, AJ, 115, 535

Cardelli, J. A., Clayton, G. C., & Mathis, J. S. 1989, ApJ, 345, 245

Carollo, C. M., Danziger, I. J., & Buson, L. 1993, MNRAS, 265, 553

Ciardullo, R. 1995, in I.A.U. Highlights of Astronomy # 10, ed. I. Appenzeller (Dordrecht: Kluwer), 507

Ciardullo, R., & Jacoby, G. H. 1992, ApJ, 388, 268

Ciardullo, R., & Jacoby, G. H. 1999, ApJin press

Ciardullo, R., Jacoby, G. H., Ford, H. C., & Neill, J. D. 1989, ApJ, 339, 53 (CJFN)

Ciardullo, R., Rubin, V. C., Ford, W. K., Jr., Jacoby, G. H., & Ford, H. C. 1988, AJ, 95, 438

Clegg, R. E. S. 1992, in IAU Symposium, 155, Planetary Nebulae, ed. R. Weinberger & A. Acker (Kluwer, Dordrecht), 549

Davidge, T. J. 1997, AJ, 113, 985

Davies, R. L., Sadler, E. M., & Peletier, R. F. 1993, MNRAS, 262, 650

Dennefeld, M., & Kunth, D. 1981, AJ, 86, 989

Dopita, M. A., Jacoby, G. H., & Vassiliadis, E. 1992, ApJ, 389, 27

Dopita, M. A., & Meatheringham, S. J. 1991a, ApJ, 367, 115

Dopita, M. A., & Meatheringham, S. J. 1991b, ApJ, 377, 480

Dopita, M. A., Vassiliadis, E., Wood, P. R., Meatheringham, S. J., Harrington, J. P., Bohlin, R. C., Ford, H. C., Stecher, T. P., & Maran, S. P. 1997, ApJ, 474, 188

Edvardsson, B., Andersen, J., Gustaffson, B., Lambert, D. L., Nissen, P. E., & Tomkin, J. 1993, A&A, 275, 101

Ferguson, H. et al. 1991, ApJ, 382, L69

Ferguson, J. W., & Ferland, G. J. 1997, ApJ, 479, 363

Ferland, G. J., Korista, K. T., Verner, D. A., Ferguson, J. W., Kingdon, J. B., & Verner, E. M. 1998, PASP, 110, 761

Ford, H. C., & Jacoby, G. H. 1978, ApJS, 38, 351

Ford, H. C., Jacoby, G. H., Ciardullo, R., Hui, X., Ptak, A. 2000, in preparation (FJCHP)

Ford, H. C., Jacoby, G., & Jenner, D. C. 1977, ApJ, 213, 18

Forestini, M., & Charbonnel, C. 1997, A&AS, 123, 241

Freedman, W. 1989, AJ, 98, 1285

Freedman, W. L., & Madore, B. F. 1990, ApJ, 365, 186

Gratton, R., Carretta, E., Matteucci, F., & Sneden, C. 1996, in Formation of the Galactic Halo .... Inside and Out, ASPC 92, ed. H. Morrison & A. Sarajedini (San Francisco: Astronomical Society of the Pacific), 307

Greggio, L., & Renzini, A. 1990, ApJ, 364, 35

Grevesse, N., & Anders, E. 1989, in AIP Conf. Proc. 183, Cosmic Abundances of Matter, Am. Inst. Phys., New York, 1

Grevesse, N., Lambert, D. L., Sauval, A. J., Van Dishoeck, E. F., Farmer, C. B., & Norton, R. H. 1990, A&A, 232, 225

Grevesse, N., Lambert, D. L., Sauval, A. J., Van Dishoeck, E. F., Farmer, C. B., & Norton, R. H. 1991, A&A, 242, 488

Grillmair, C. J., et al. 1996, AJ, 112, 1975

Henry, R. B. C. 1989, MNRAS, 241, 468

Henry, R. B. C. 1990, ApJ, 356, 229

van den Hoek, L. B., & Groenwegen, M. A. T. 1997, A&AS, 123, 241

Holland, S., Fahlman, G. G., & Richer, H. B. 1996, AJ, 112, 1035

van der Hucht, K. A., Conti, P. S., Lundström, I., & Stenholm, B. 1981, Sp.Sci., 28, 227

Jacoby, G. H. 1989, ApJ, 339, 39

Jacoby, G. H. 1996, in The Extragalactic Distance Scale, Proceedings of the ST ScI May Symposium, ed. M. Livio, M., Donahue, & N. Panagia, (Cambridge: Cambridge University Press), 197

Jacoby, G. H., & Ford, H. C. 1986, ApJ, 304, 490

Jacoby, G. H., Ford, H. C., & Ciardullo, R. 1985, ApJ, 290, 136

Jacoby, G. H., Morse, J. A., Fullton, L. K., Kwitter, K. B., & Henry, R. B. C. 1997, AJ, 114, 2611

Kaler, J. B. 1995, in I.A.U. Highlights of Astronomy # 10, ed. I. Appenzeller (Dordrecht: Kluwer), 480

Kennicutt, R. C. et al. 1998, ApJ, 498, 181

Kingsburgh, R. L., & Barlow, M. J. 1994, MNRAS, 271, 257

King, J. R. 1994, AJ, 107, 350

McElroy, D. B. 1983, 1983, ApJ, 270, 485

McWilliam, A. 1997, ARA&A, 35, 503

McWilliam, A., & Rich, M. R. 1994, ApJS, 91, 749

Méndez, R. H., Kudritzki, R. P., Jacoby, G. H., & Ciardullo, R. 1993, A&A, 275, 534

Mould, J., & Kristian, J. 1986, ApJ, 305, 59

Mowlavi, N., Meynet, G., Maeder, A., Schaerer, D., & Charbonnel, C. 1998, A&A, 335, 573

Oke, J. B. 1974, ApJS, 27, 21

Olszewski, E. W., Suntzeff, N. B., & Mateo, M. 1996, ARA&A, 34, 511

Osterbrock, D. E. 1989, Astrophysics of Gaseous Nebulae and Active Galactic Nuclei (Mill Valley: University Science Books)

Peimbert, M., & Torres-Peimbert, S. 1983, in IAU Symp. 103, Planetary Nebulae, ed. Flower, D. R., (Reidel: Dordrecht), 233

Ratag, M. A., Pottasch, S. R., Dennefeld, M., & Menzies, J. 1997, A&AS, 126, 297

Reitzel, D. B., Guhathakurta, P., & Gould, A. 1998, AJ, 116, 707

Richer, M. G. 1993, ApJ, 415, 240

Richer, M. G., Mc Call, M. L., & Arimoto, N. 1997, A&AS, 122, 215

Richer, M. G., Stasińska, G., & Mc Call, M. L. 1998, A&A, in press (RSM)

Schönberner, D. 1983, ApJ, 272, 708

Spinrad, H. & Taylor, B. 1971, ApJS, 22, 445

Stasińska, G., Richer, M. G., & Mc Call, M. L. 1998, A&A, 336, 667 (SRM)

Stone, R. P. S. 1977, ApJ, 218, 767

Tylenda, R., Acker, A., & Stenholm, B. 1993, A&AS, 102, 595

van Hoof, P. A. M., & Van de Steene, G. C. 1997, in Photoionization Studies of Nebulae, Ph.D. thesis by P. A. M. van Hoof (Groningen: Rijkuniversiteit), 7

Vassiliadis, E., & Wood, P. R. 1994, ApJS, 92, 125

Vazdekis, A., Peletier, R. F., Beckman, J. E., & Casuso, E. 1997, ApJS, 111, 203

Walsh, J. R., Dudziak, G., Minniti, D., & Zijlstra, A. A. 1997, ApJ, 487, 651

Walsh, J. R., Walton, N. A., Jacoby, G. H., & Peletier, R. F. 1998, A&A, submitted

Weidemann, V., & Koester, D. 1983, A&A, 121, 77

Worthey, G., Faber, S. M., & Gonzalez, J. J. 1992, ApJ, 398, 69 (WFG)

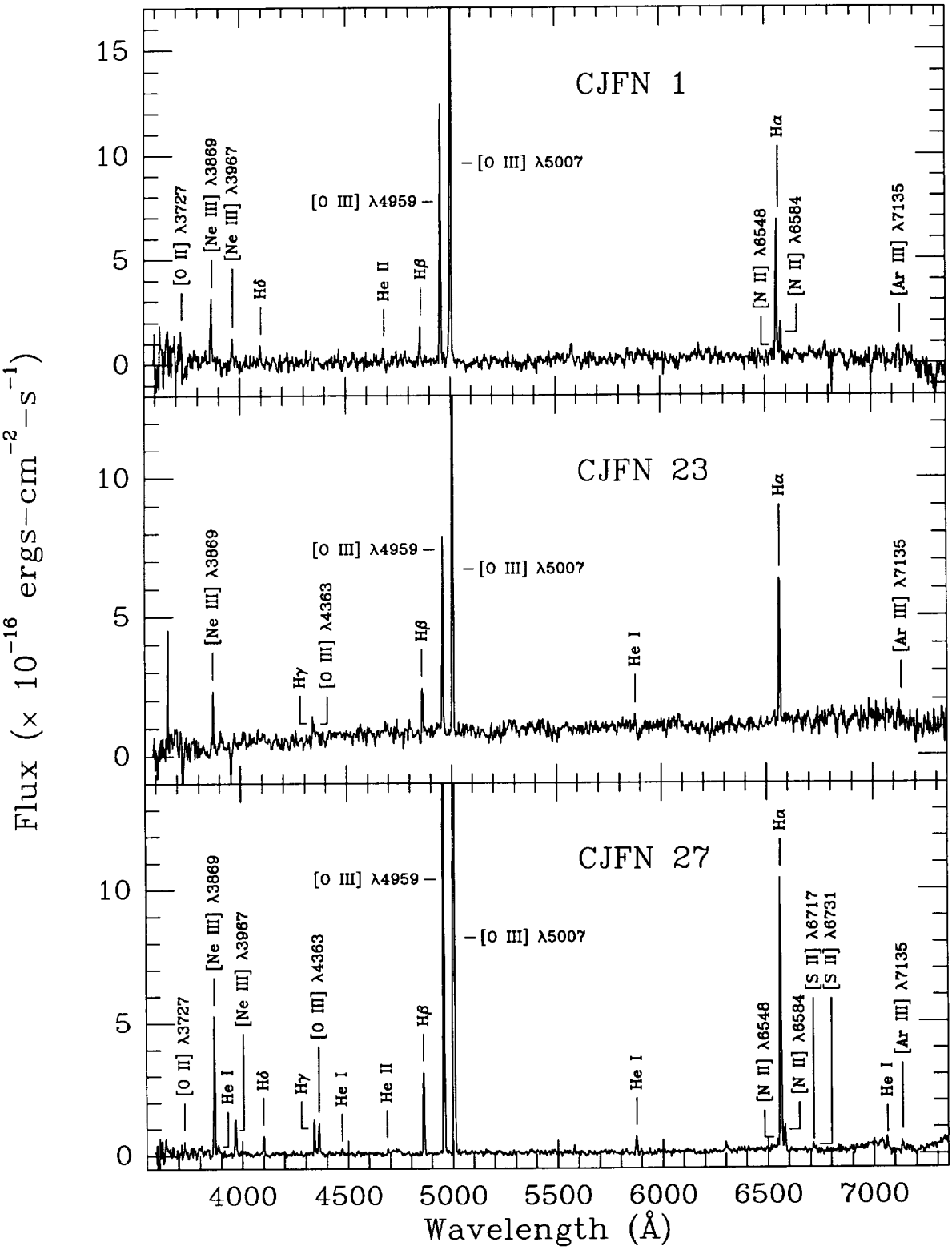

Fig. 1.— Spectra of the bulge PNe, CJFN 1, 23, and 27. The detected lines of astrophysical interest are labeled. In some spectra, a residual from the sky subtraction is seen at λ5577 due to the very strong [OI] night sky line.

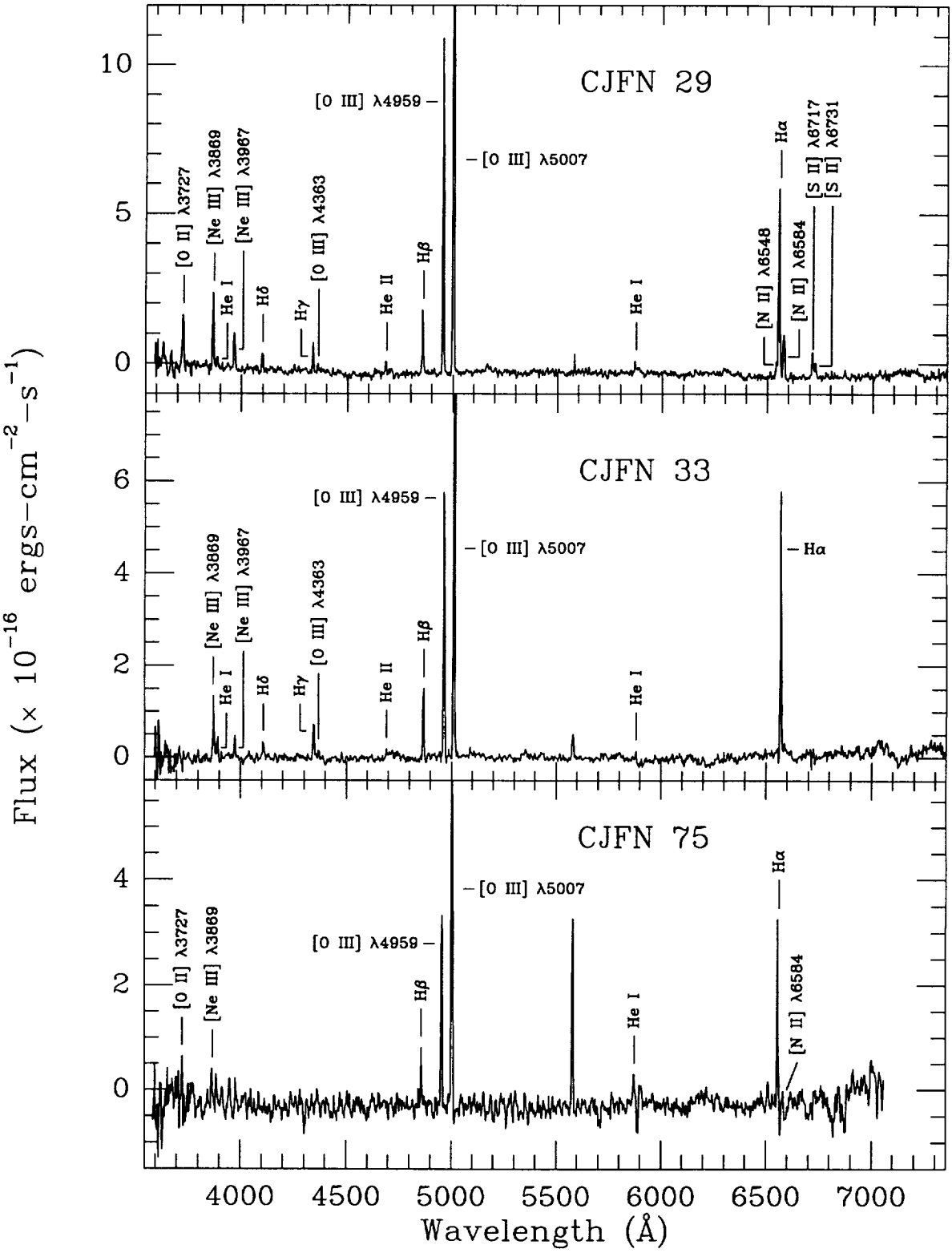

Fig. 1., cont'd.— Spectra of the bulge PNe, CJFN 29, 33, and 75. The [OI] λ5577 residual from the sky is especially evident for CJFN 75.

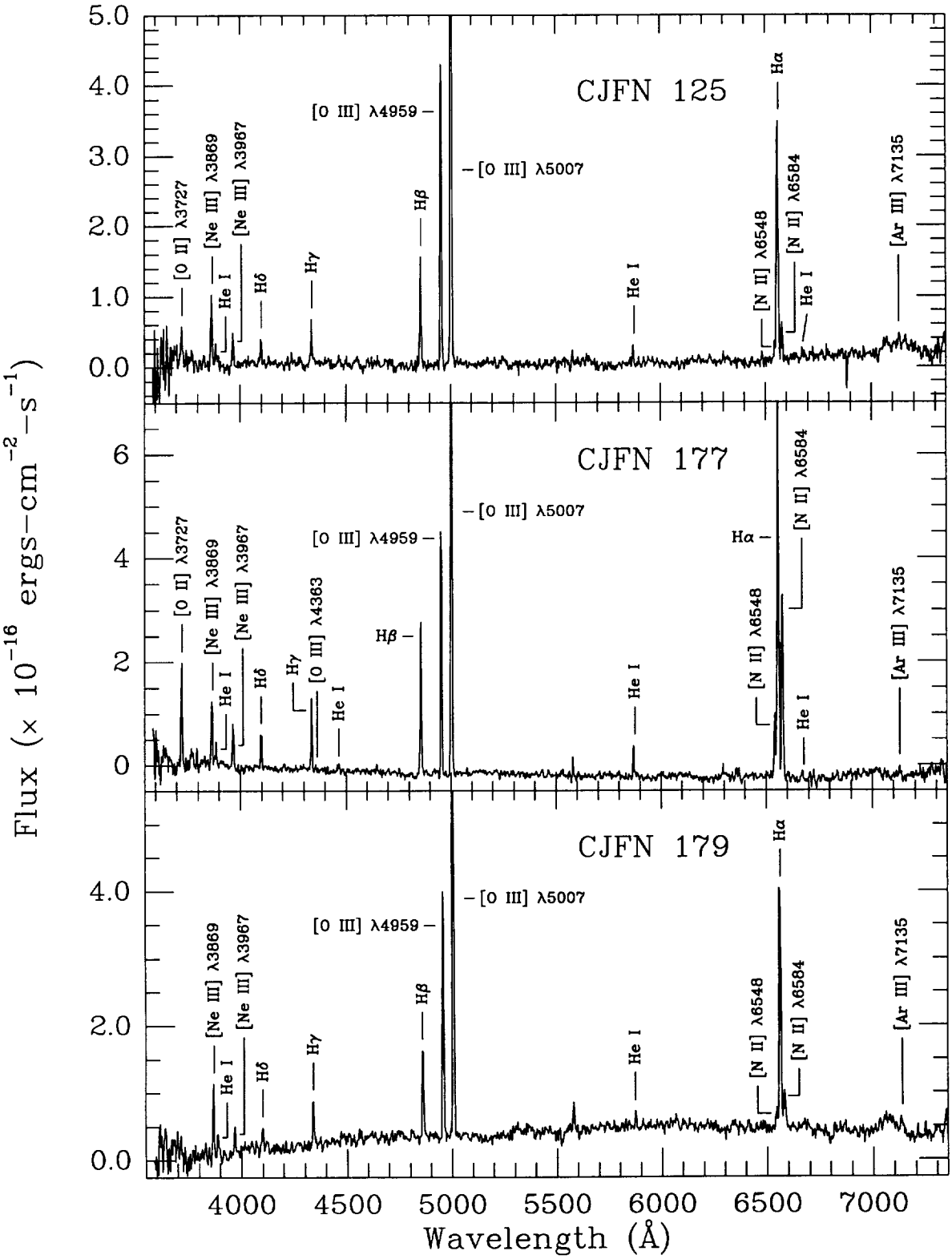

Fig. 1., cont'd.— Spectra of the bulge PNe, CJFN 125, 177, and 179

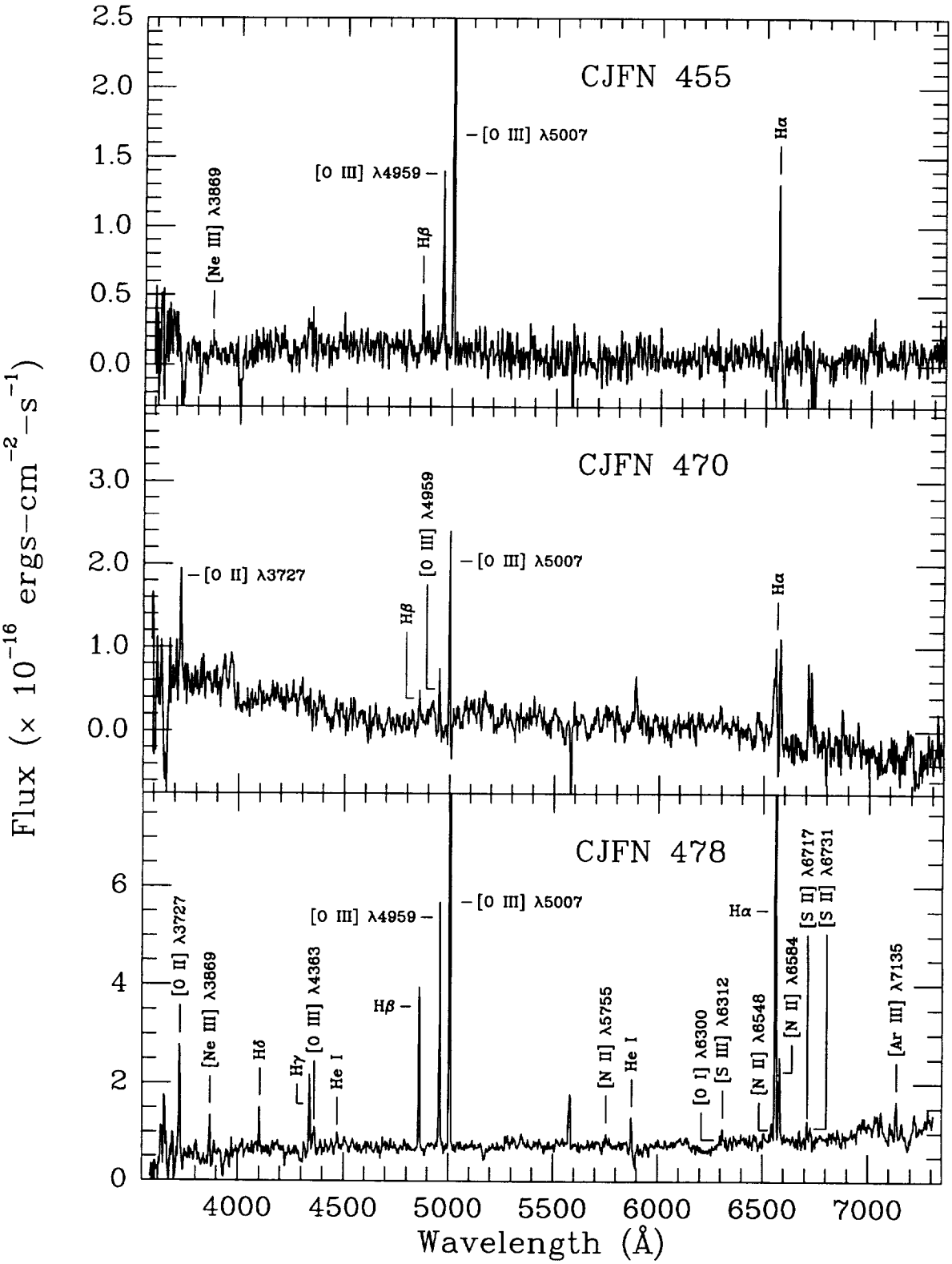

Fig. 1., cont'd.— Spectra of the bulge PNe, CJFN 455, 470, and 478

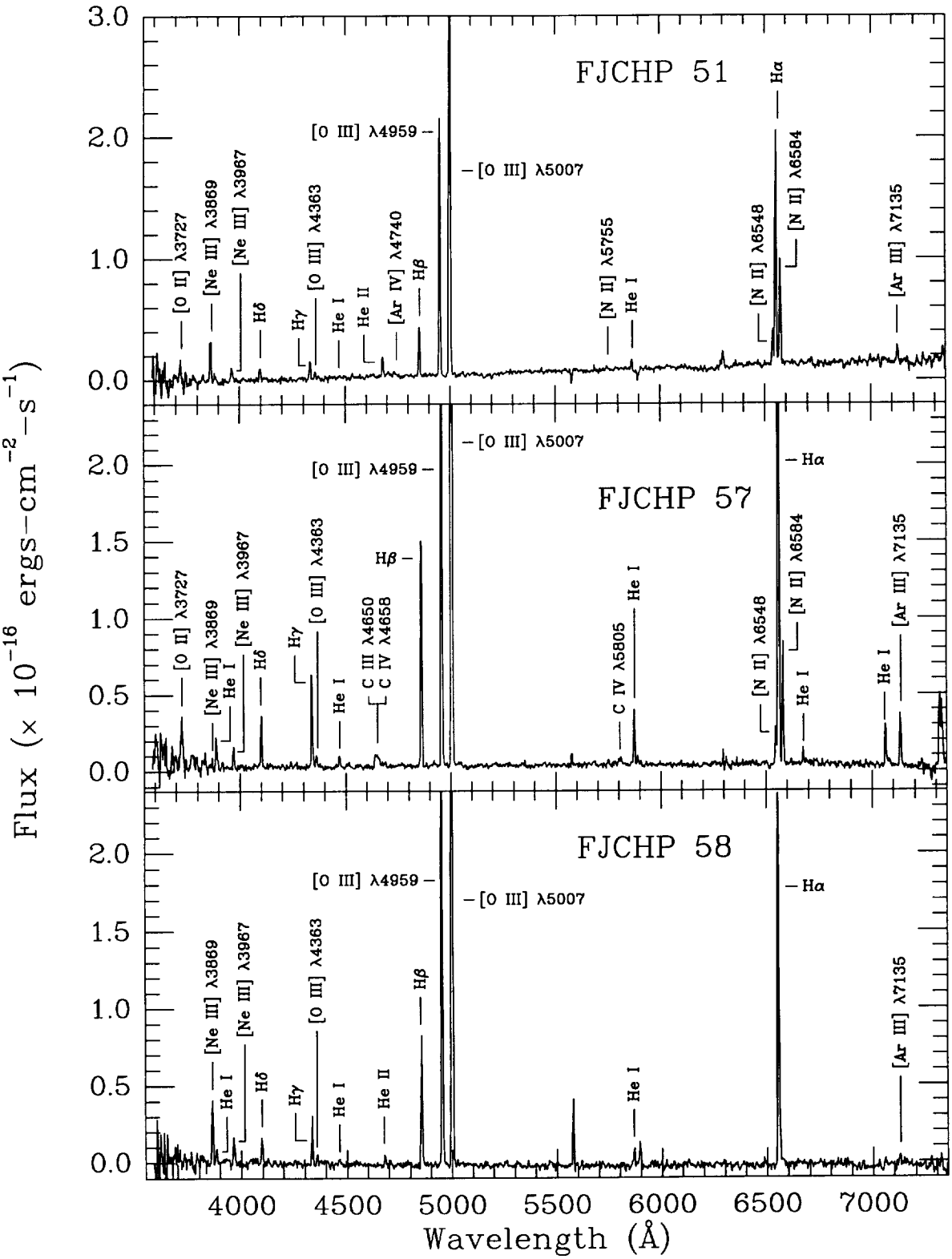

Fig. 2.— Spectra of the 3 disk PNe, FJCHP 51, FJCHP 57, and FJCHP 58.

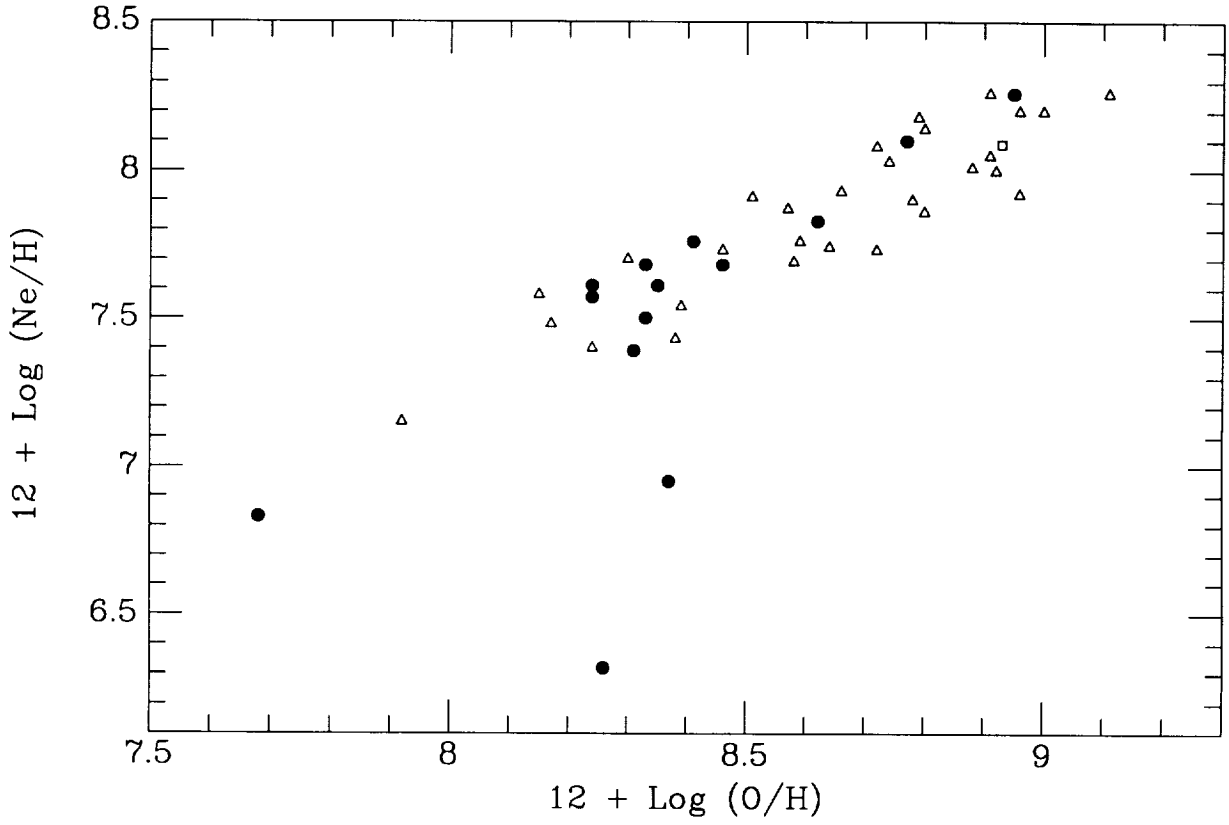

Fig. 3.— The correlation between Ne/H and O/H is evident and follows the same function as that seen by Henry (1989). The solid points represent the PNe from this study. Open triangles are those reported by SRM for their M31 PNe. The solid square is the Sun. The two objects that fall off the relationship are FJCHP 57, a probable halo PN with the lowest neon abundance in the sample, and CJFN 455, which has a marginal detection for neon.

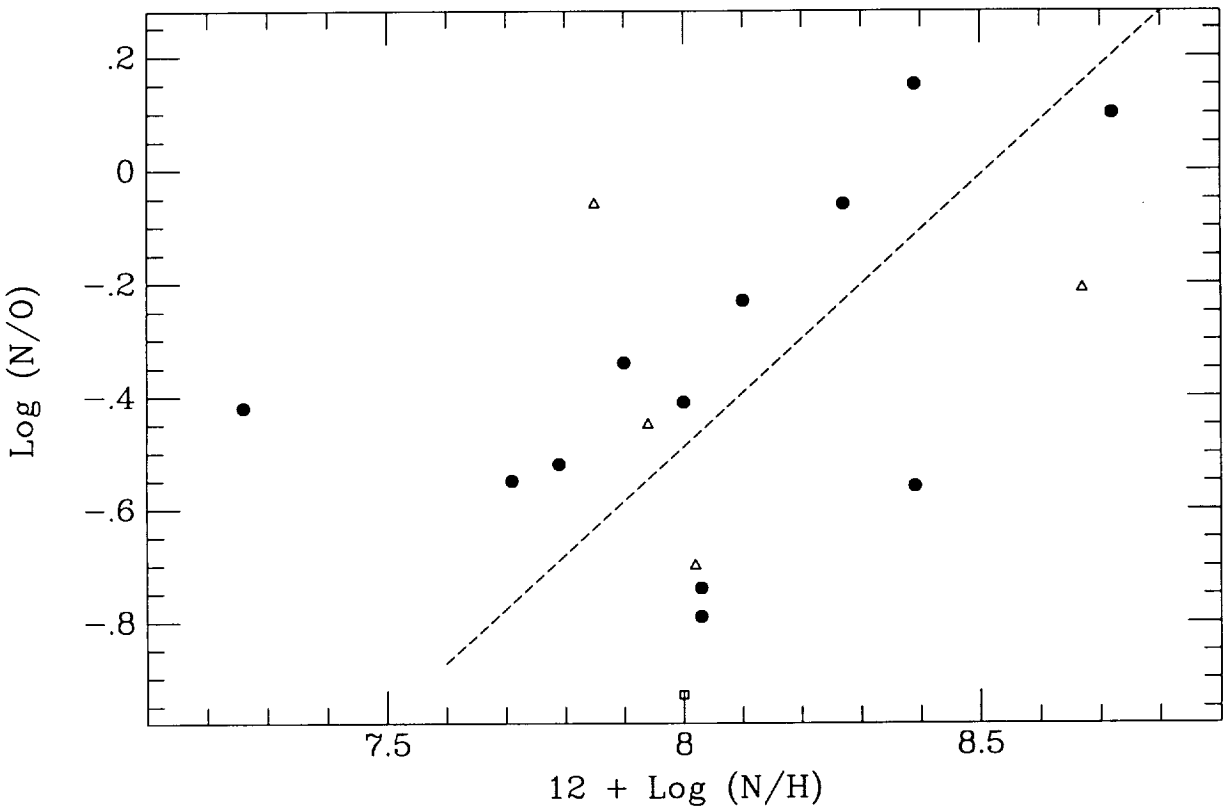

Fig. 4.— The relationship between N/O and N/H. The dashed line shows the fit to the Galactic data determined by Henry (1990). The point that falls off the line to the left, with the lowest N/H, is CJFN 478, a possible halo PN. Symbols are the same as in Figure 3.

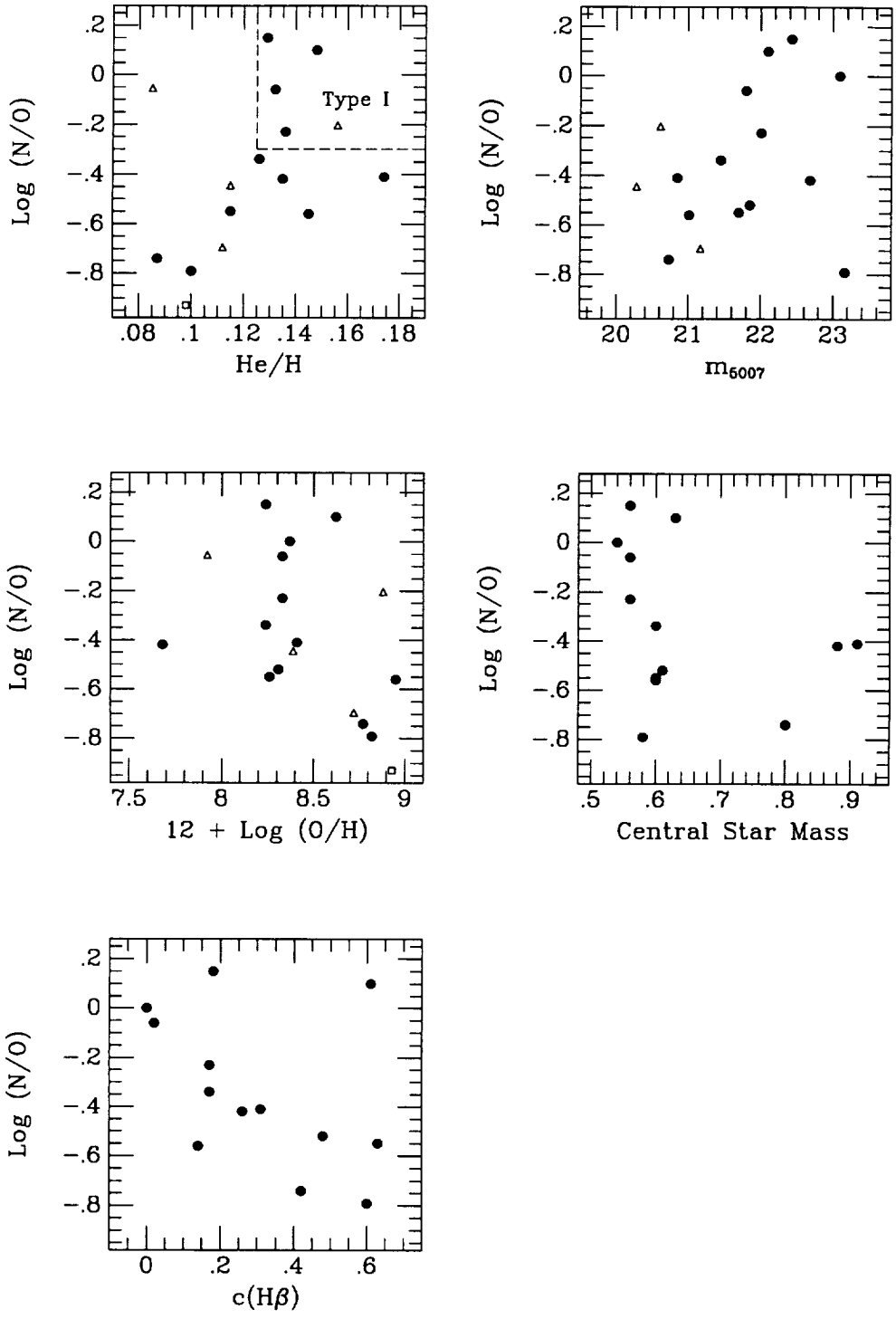

Fig. 5.— A variety of N/O relationships: (a) N/O vs He/H with the Type I regime as defined by Peimbert & Torres-Peimbert (1983) indicated; (b) N/O vs O/H showing a mild, if any, anti-correlation; (c) N/O vs the extinction parameter, $c(\mathrm{H}\beta)$; (d) N/O vs m_{5007}, and (e) N/O vs central star mass. Symbols are the same as in Figure 3.

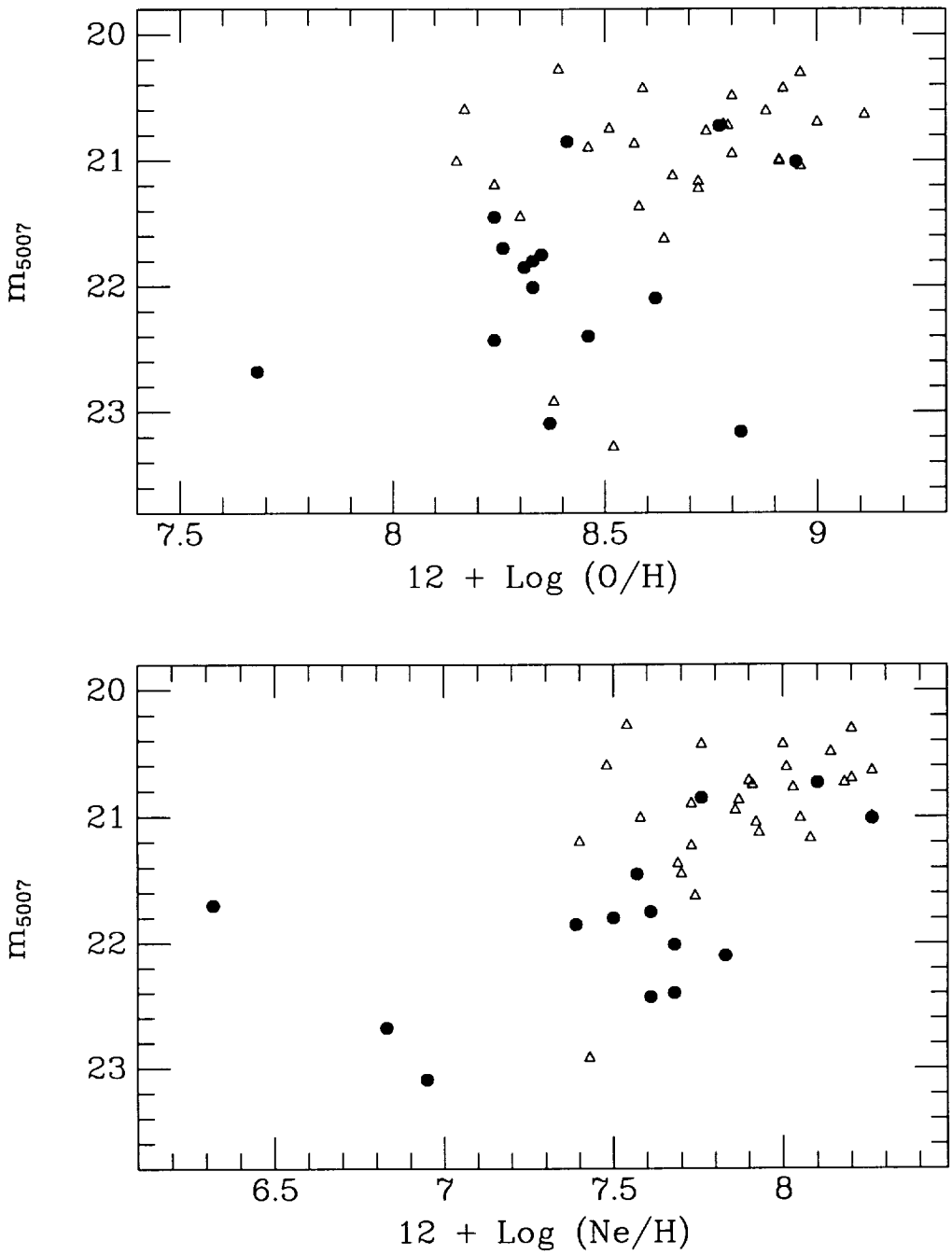

Fig. 6.— The relationships between apparent PN brightness, m_{5007}, and the oxygen and neon abundances. The upper envelopes are nearly flat as abundance changes, indicating near-independence of PN maximum luminosity with metallicity. Symbols are the same as in Figure 3.

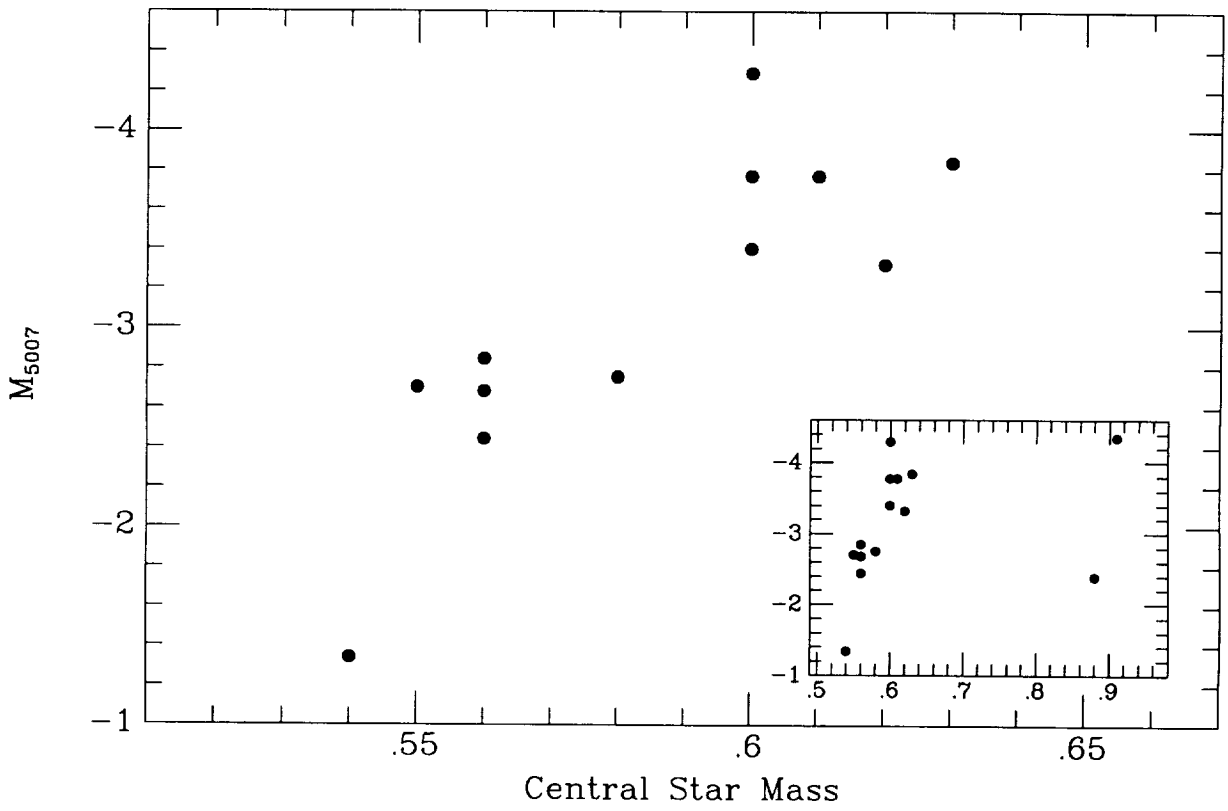

Fig. 7.— The absolute magnitude at [OIII] λ5007 (corrected for the measured extinction) correlates with central star mass, at least for the low-to-moderate mass stars. The correlation may break down at higher masses (see inset).

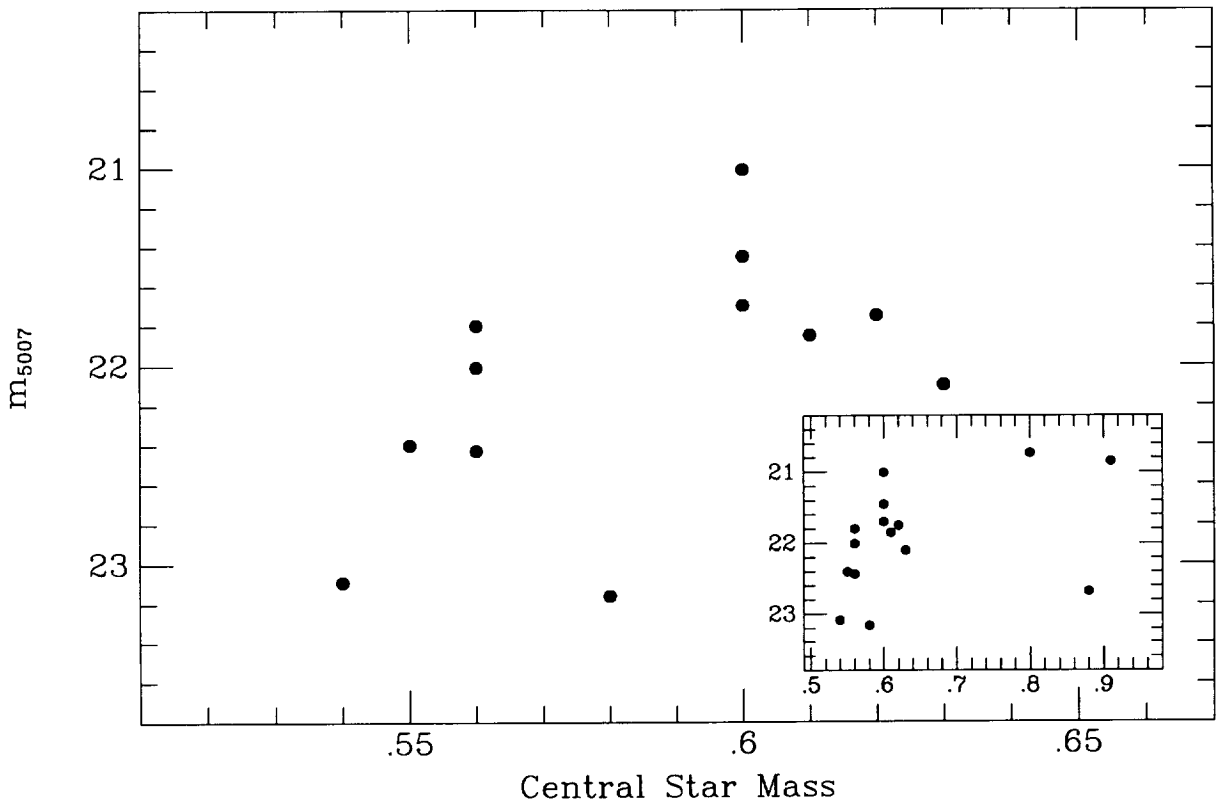

Fig. 8.— The apparent magnitude at [OIII] λ5007 correlates, though poorly, with central star mass. Again the high mass regime (see inset) shows even less correlation.

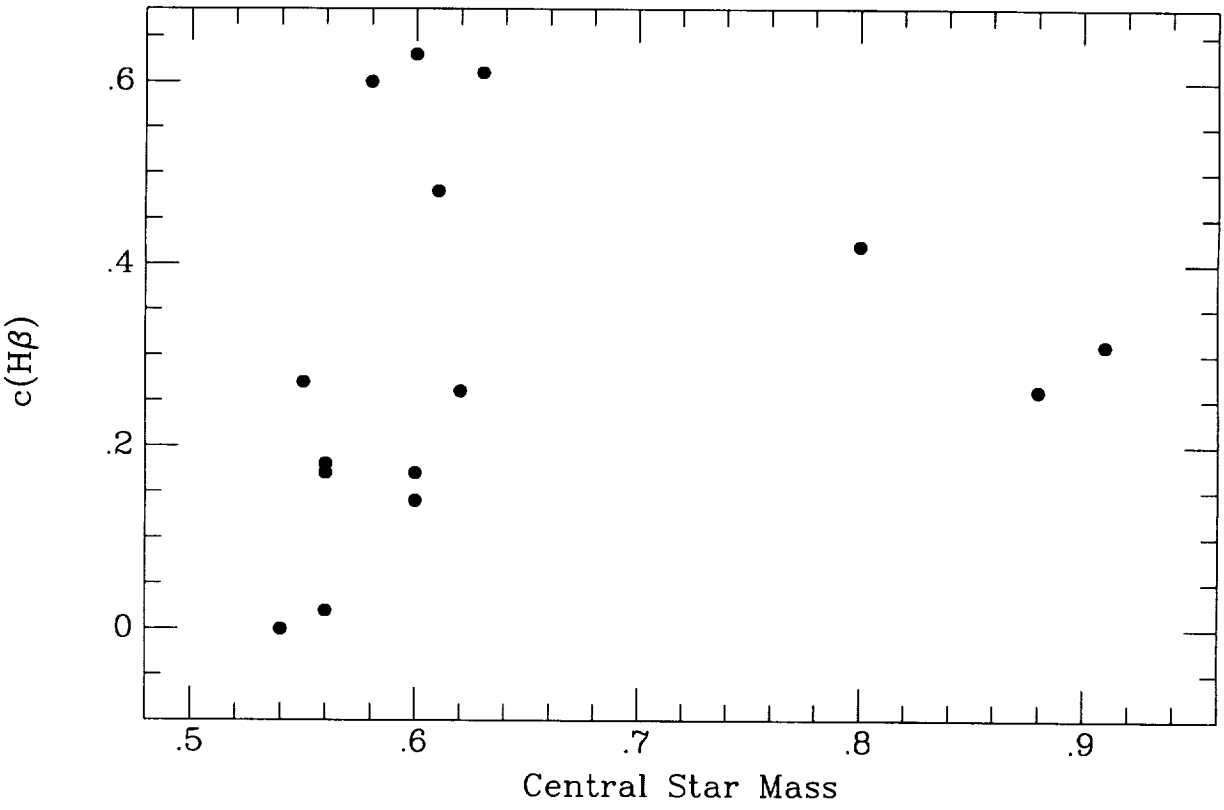

Fig. 9.— A correlation between extinction and central star mass must exist in order to explain the good and poor correlations seen between absolute and apparent magnitudes in the previous figures.

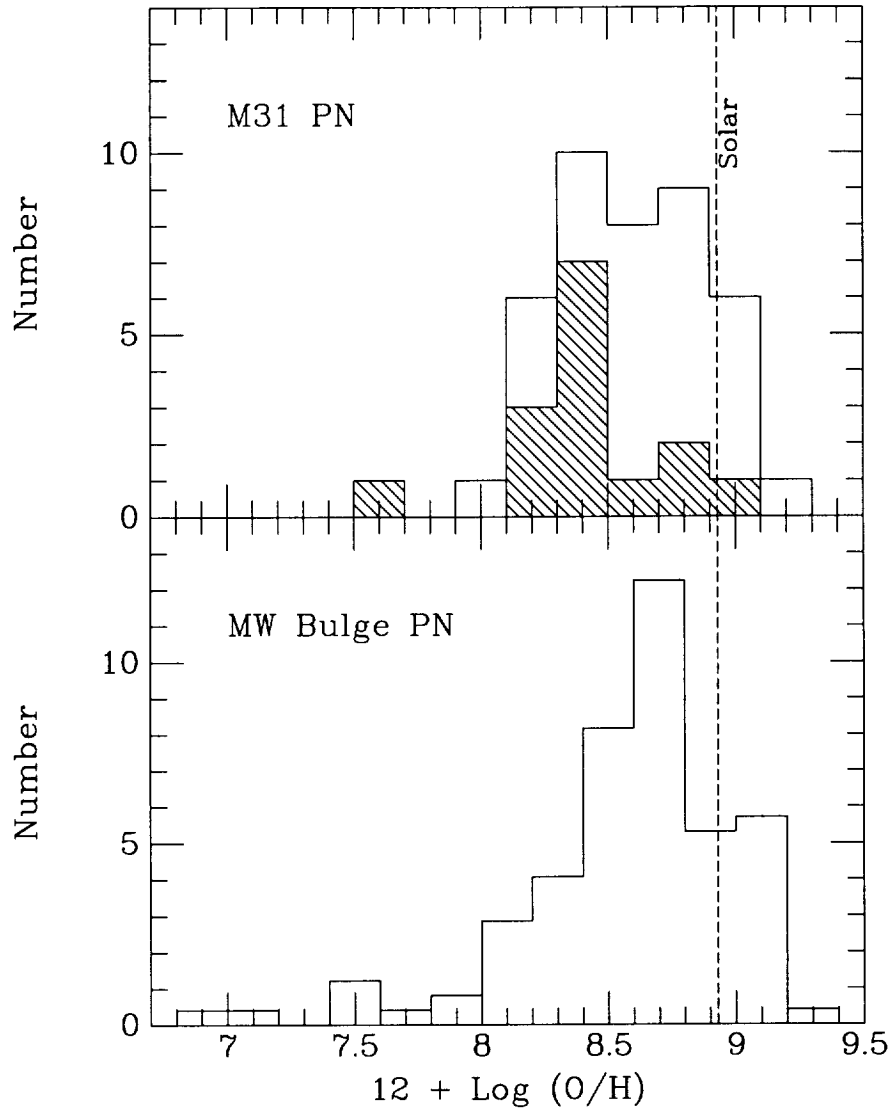

Fig. 10.— The upper panel shows the distribution of oxygen abundances for the 15 PNe in our sample (hatched) and in the total sample (including the SRM data). The solar oxygen value is indicated by the vertical dashed line. The SRM sample draws from a somewhat more oxygen-rich population than our sample, presumably because of that sample's bias toward's [OIII]-bright PNe. The lower panel shows the oxygen abundance distribution for the Galactic bulge PNe from Ratag et al. (1997). That sample of 103 PNe has been normalized to match the same total number (42) of PNe in the upper sample (ours plus SRM). Clearly, few PNe in any sample have super-solar oxygen abundances.

TABLE 1. Summary of Observations

Setup	Exp (hrs)	Begin HA	End HA	ID[a]	α(2000)	δ(2000)	m_{5007}
1	6.5	−3 16	+3 29	1	00 42 46.10	41 16 40.9	20.73
1				9	00 42 45.15	41 16 05.4	21.47
1				23	00 42 48.89	41 16 55.5	21.45
1				27	00 42 57.93	41 16 21.2	20.85
1				29	00 42 53.48	41 17 33.9	21.01
1				33	00 42 57.75	41 18 48.3	21.75
1				75	00 42 51.31	41 15 56.6	21.85
1				125	00 43 05.20	41 17 38.1	21.80
1				177	00 43 02.37	41 16 49.8	22.01
1				179	00 43 03.69	41 17 37.6	22.43
1				455	00 42 46.02	41 18 24.4	23.09
1				470	00 42 52.75	41 16 47.4	23.16
1				478	00 42 55.23	41 17 12.1	22.68
2	6.0	−4 04	+3 11	F51	00 40 04.13	40 21 14.1	22.15
2				F57	00 40 14.21	40 23 23.5	21.70
2				F58	00 40 15.26	40 24 13.0	22.36

[a]All PN identifications are from CJFN, except for F51, F57, and F58, which are from FJCHP

TABLE 2. M31 PN Reddening-Corrected Line Strengths: Observed and Modeled[a]

λ	Ion	1[b]	23	27	29	33	75	125	177	179	455	470	478	F51	F57	F58
3727	[O II]	1.37	...	0.14	1.28	...	0.81	0.32	0.78	...	...	7.04	1.06	0.49	0.40	...
		1.36	0.36	0.09	1.28	0.22	0.79	0.29	0.78	0.22	0.90	7.03	1.12	0.49	0.41	0.17
3869	[Ne III]	2.10	1.24	1.99	1.29	0.96	0.82	0.55	0.42	0.74	0.22	...	0.36	1.13	0.03	0.58
		2.12	1.24	1.98	1.29	0.96	0.81	0.54	0.43	0.74	0.23	1.12	0.35	1.12	0.03	0.57
3889	He I + H I	...	...	0.17	0.19	0.35	...	0.15	0.14	0.25	...	...	...	...	0.14	0.18
		0.16	0.20	0.15	0.16	0.15	0.20	0.20	0.16	0.20	0.21	0.20	0.25	0.19	0.14	0.16
3969	[Ne III] + H I	0.66	...	0.55	0.71	0.37	...	0.29	0.31	0.27	...	...	...	0.49	0.14	0.28
		0.80	0.54	0.77	0.55	0.45	0.41	0.33	0.39	0.40	0.23	0.50	0.27	0.51	0.12	0.34
4101	H I	0.44	...	0.27	0.31	0.32	...	0.20	0.24	0.24	...	...	0.23	0.36	0.26	0.23
		0.27	0.27	0.27	0.27	0.27	0.26	0.27	0.27	0.27	0.27	0.27	0.26	0.27	0.27	0.27
4340	H I	...	0.62	0.43	0.49	0.62	...	0.43	0.47	0.56	...	...	0.55	0.46	0.52	0.37
		0.48	0.48	0.48	0.48	0.48	0.48	0.48	0.48	0.48	0.48	0.48	0.47	0.48	0.48	0.48
4363	[O III]	...	0.23	0.40	0.10	0.15	...	...	0.02	...	...	...	0.17	0.16	0.06	0.09
		0.27	0.20	0.38	0.08	0.14	0.23	0.08	0.03	0.07	0.13	0.04	0.12	0.18	0.07	0.09
4471	He I	...	...	0.06	...	...	...	...	0.06	...	...	...	0.09	0.09	0.06	0.05
		0.02	0.05	0.08	0.06	0.02	0.06	0.06	0.07	0.06	0.06	0.04	0.06	0.05	0.06	0.04
4686	He II	0.44	...	0.07	0.20	0.04	...	...	...	...	...	...	...	0.45	...	0.09
		0.45	0.11	0.07	0.20	0.04	0.13	0.06	0.00	0.06	0.05	0.26	0.05	0.45	0.00	0.09
4740	[Ar IV]	...	...	...	...	...	...	...	...	...	...	...	...	0.10	...	...
		0.11	0.07	0.04	0.01	0.01	0.02	0.01	0.00	0.02	0.03	0.00	0.03	0.07	0.01	0.01
4861	H I	1.00	1.00	1.00	1.00	1.00	1.00	1.00	1.00	1.00	1.00	1.00	1.00	1.00	1.00	1.00
		1.00	1.00	1.00	1.00	1.00	1.00	1.00	1.00	1.00	1.00	1.00	1.00	1.00	1.00	1.00
4959	[O III]	6.22	4.07	5.28	4.78	3.78	4.41	2.86	1.53	2.50	3.38	2.24	1.30	5.02	2.29	3.39
		6.64	4.18	5.63	5.11	3.99	4.51	2.95	1.57	2.53	3.33	2.48	1.46	5.29	2.37	3.50
5007	[O III]	19.07	12.07	16.22	14.85	11.53	13.22	8.50	4.54	7.31	9.68	7.15	4.13	15.24	6.90	10.17
		19.17	12.08	16.27	14.76	11.53	13.03	8.51	4.52	7.32	9.61	7.17	4.22	15.26	6.85	10.10

TABLE 2. (continued)

λ	Ion	1[b]	23	27	29	33	75	125	177	179	455	470	478	F51	F57	F58
5755	[N II]	...	...	...	...	...	...	...	...	...	...	...	0.05	0.03	...	...
		0.02	0.01	0.02	0.01	0.00	0.02	0.01	0.02	0.01	0.02	0.04	0.01	0.04	0.01	0.00
5876	He I	...	0.15	0.22	0.18	0.06	0.76	0.16	0.19	0.16	...	1.30	0.16	0.14	0.16	0.12
		0.06	0.15	0.22	0.18	0.06	0.18	0.17	0.18	0.16	0.16	0.12	0.16	0.14	0.15	0.12
6300	[O I]	...	...	...	...	...	...	0.06	...	...	...	...	0.03	...	...	...
		0.04	0.00	0.02	0.02	0.00	0.00	0.00	0.01	0.00	0.00	0.42	0.02	0.00	0.00	0.00
6312	[S III]	...	...	...	...	...	...	...	...	...	...	...	0.05	...	...	...
		0.02	0.04	0.20	0.07	0.04	0.04	0.03	0.03	0.05	0.04	0.05	0.03	0.03	0.02	0.03
6548	[N II]	0.29	...	0.07	0.29	...	...	0.17	0.43	0.21	...	...	0.10	0.45	0.11	...
		0.25	0.09	0.09	0.27	0.03	0.22	0.15	0.44	0.18	0.24	0.93	0.17	0.48	0.11	0.02
6563	H I	2.85	2.85	2.85	2.85	2.85	2.85	2.85	2.85	2.85	2.65	2.85	2.85	2.85	2.85	2.85
		2.85	2.83	2.76	2.86	2.82	2.88	2.83	2.86	2.83	2.84	2.87	3.06	2.83	2.87	2.84
6583	[N II]	0.73	...	0.27	0.82	...	0.63	0.44	1.31	0.55	...	2.74	0.49	1.42	0.31	...
		0.72	0.27	0.28	0.80	0.10	0.65	0.45	1.31	0.54	0.72	2.76	0.50	1.40	0.31	0.06
6678	He I	...	...	...	...	...	...	0.06	0.07	...	...	...	...	...	0.04	...
		0.02	0.04	0.06	0.05	0.02	0.05	0.05	0.05	0.05	0.04	0.03	0.05	0.04	0.04	0.04
6717	[S II]	...	...	0.07	0.51	...	...	...	...	...	...	2.08	0.10	...	...	...
		0.03	0.02	0.03	0.49	0.02	0.05	0.03	0.06	0.03	0.04	2.08	0.12	0.06	0.01	0.02
6731	[S II]	...	...	0.04	0.29	...	...	...	...	...	...	1.89	0.11	...	...	...
		0.07	0.04	0.07	0.42	0.03	0.09	0.05	0.10	0.05	0.08	1.66	0.11	0.03	0.03	0.04
7065	He I	...	...	0.12	...	...	...	...	...	...	...	...	...	...	0.12	...
		0.05	0.13	0.27	0.09	0.04	0.18	0.09	0.11	0.08	0.12	0.02	0.06	0.10	0.12	0.08
7135	[Ar III]	0.31	0.23	0.07	...	...	...	0.09	0.03	0.17	...	...	0.18	0.23	0.14	0.06
		0.31	0.24	0.07	0.03	0.04	0.08	0.09	0.03	0.17	0.26	0.03	0.18	0.22	0.15	0.06
c		0.42	0.17	0.31	0.14	0.26	0.48	0.02	0.17	0.20	0.00	0.60	0.26	0.61	0.63	0.27
Log L_{5007}		36.48	35.94	36.32	36.09	35.91	36.09	35.65	35.70	35.58	35.12	35.68	35.54	36.13	36.30	35.68

[a]Observed line strengths are given first, followed on the next line by the strengths predicted by the CLOUDY models.
[b]All PN identifications are from CJFN, except for F51, F57, and F58, which are from FJCHP

TABLE 3. M31 PN Nebula and Central Star Parameters

PN[a]	He[b]/H	C[c]/H	N[d]/H	O/H	Ne/H	S/H	Ar/H	T_{eff}, K	Log L/L$_\odot$	Mass, M$_\odot$	T_e^e, K	N_e^e, cm^{-3}	Radius, pc
1	0.087	8.70	8.03	8.77	8.10	...	6.57	140000	4.16	0.80	14600	8800	0.058
23	0.126	8.10	7.90	8.24	7.57	...	6.23	85000	3.70	0.60	14300	5700	0.061
27	0.174	8.10	8.00	8.41	7.76	7.54	5.82	67000	4.35	0.91	14000	89000	0.012
29	0.145	8.85	8.39	8.95	8.26	7.70	...	107000	3.66	0.60	9000	550	0.462
33	0.050	8.62	...	8.35	7.61	...	...	68000	3.87	0.62	12500	4200	0.068
75	...	8.20	7.79	8.31	7.39	...	...	90000	3.79	0.61	14400	9200	0.048
125	0.132	8.30	8.27	8.33	7.50	...	5.90	80000	3.37	0.56	11400	2300	0.094
177	0.136	8.74	8.10	8.33	7.68	...	5.51	55000	3.52	0.56	9900	4600	0.073
179	0.129	8.30	8.39	8.24	7.61	...	6.18	80000	3.37	0.56	11600	2300	0.092
455	...	8.20	...	8.37	6.95	...	...	75000	2.78	0.54	12800	5700	0.034
470	0.100	8.82	8.03	8.82	...	7.38	...	132000	3.36	0.58	9500	150	0.616
478	0.135	6.80	7.26	7.68	6.83	6.24	5.90	75000	4.30	0.88	16400	460	0.360
F51	0.148	8.95	8.72	8.62	7.83	6.90	6.42	136000	3.79	0.63	13000	5900	0.062
F57	0.115	8.64	7.71	8.26	6.32	...	6.08	58000	3.77	0.60	11300	11200	0.057
F58	0.100	8.80	...	8.46	7.68	...	5.81	90000	3.22	0.55	11100	7000	0.042
Average	0.121	8.58	8.19	8.50	7.71	7.37	6.15						
Median	0.129	8.62	8.03	8.35	7.61	7.38	6.00						
σ	0.031	0.23	0.28	0.23	0.29	0.26	0.24						
Solar[f]	0.098	8.60	8.00	8.93	8.09	7.21	6.56						
MW PN	0.115	8.74	8.35	8.68	8.09	6.92	6.39						
Orion	0.100	8.53	7.83	8.60	7.91	6.93	6.35						
LMC PN	0.105	8.74	8.07	8.44	7.70	6.51	5.93						
SMC PN	0.107	8.78	7.84	8.24	7.41	6.48	5.62						
Sag PN	0.106		7.41	8.30	7.54	6.40	5.82						
Cena A PN	...	...	8.02	8.39	...	7.10	...						
ΔICF[g]	-0.003		0.11	0.08	0.05	0.16	-0.13						

[a]All PN identifications are from CJFN, except for F51, F57, and F58, which are from FJCHP

[b]Helium abundances are given by number relative to hydrogen

[c]Carbon abundances, given as 12 + Log (C/H), are assumed values (see text)

[d]Nitrogen, oxygen, neon, sulfur, and argon abundances are given as 12 + Log (X/H)

[e]T_e and N_e are the volume-averaged values within the nebulae

[f]Solar abundances are taken from Clegg's (1992) summary of Grevesse & Anders (1989), Grevesse et al. (1990), Grevesse et al. (1991), Milky Way PN from Kingsburg and Barlow (1994), Orion from Rubin et al. (1991), LMC and SMC from Clegg (1992), Sagittarius Dwarf from Walsh et al. (1997), Cen A from Walsh et al. (1998)

[g]Average difference between CLOUDY and ICF-based abundances